Available online at www.sciencedirect.com
SCIENCE DIRECT®
ELSEVIER
International Journal of Solids and Structures 43 (2006) 5267–5294
INTERNATIONAL JOURNAL OF SOLIDS and STRUCTURES
www.elsevier.com/locate/ijsolstr

Transient response of a thin cylinder with local material inhomogeneity

Michael El-Raheb *

ATK Mission Research, Laguna Hills, CA, United States

Received 21 April 2005
Available online 1 July 2005

Abstract

Analyzed is transient response of a thin cylinder with a local material inhomogeneity to a pulse of short duration. The Galerkin method is utilized to solve the inhomogeneous dynamic equations with the eigenfunctions of the homogeneous cylinder serving as trial functions. Also treated is response of the limiting cases of a disk and of a ring with the same local inhomogeneity. All limiting cases yield to analysis when modulus E is approximated by segments of constant E along the radius for the disk and circumference for the ring. Transfer matrices relating variables at the two ends of a segment combine to satisfy continuity of variables at interfaces of segments. Curvature and axial dependence make the cylinder unique in response properties that neither disk nor ring possess.

Keywords: Thin cylinders; Local inhomogeneity; Wave propagation

1. Introduction

Dynamic response of thin cylinders has been treated extensively. Stanton (1988), Batard and Quentin (1992), Honarvar and Sinclair (1996), Bao et al. (1997), Grinchenko (1999), and Wang and Ying (2001), treat frequency response of thin cylinders. Soldatos and Ye (1994) treat anisotropic laminated cylinders and Lin and Jen (2003) adopt the Chebyshev collocation method for the same problem. Hussein and Heyliger (1998) consider layered piezoelectric cylinders. Wang et al. (1997) utilize the Ritz method in the modal response of ring-stiffened cylinders. Um et al. (1998) derive 3-D elasticity solutions to frequency response of open cylinders. Cheung et al. (2003) analyze the 3-D vibration of solid and hollow cylinders by the

* Tel.: +1 626 7965528; fax: +1 626 5838834.
E-mail address: mertrident@earthlink.net

0020-7683/$ - see front matter
doi:10.1016/j.ijsolstr.2005.04.041

Chebyshev–Ritz method. El-Raheb and Wagner adopt transfer matrices to treat frequency response of cylinders connected to toroidal shells (1985), damped by constrained visco-elastic layers applied to the surface (1986), and acoustic radiation from thin cylinders stiffened by discrete rings and annular disks (1989a). Soldatos (1994) presents a compilation of more than 150 references on frequency response of solid and annular elastic cylinders. Very few references discuss transient response. El-Raheb and Wagner (1989b) treat wave propagation in a thin cylinder with concentrated masses attached to its surface adopting a modal approach. El-Raheb (2004) treats transient response of a thin metallic capsule made of a short cylinder capped by disks and excited by an internal pulse of short duration. Stepanishen and Janus (1990) treat transient radiation and scattering from fluid loaded cylinders. Paul and Murali (1995) determine the axisymmetric dynamic response of poro-elastic cylinders.

Many practical applications involve cylinders with local material inhomogeneity over part of the cylinder's surface. Analysis of these applications relies mostly on general–purpose computer programs like finite element, finite difference, finite volume and smooth particle hydrodynamics (SPH). These discretization techniques are necessary to solve complicated geometries and realistic material properties. For transient phenomena from external loads of short duration, these simulations may take several hours on personal workstations. To validate results from these simulations, engineers tend to simplify geometry and properties like choosing a ring, an infinite shell or a plate. Understanding the validity of these approximations is necessary since comparing results from a discretization method to flawed approximations may lead to more uncertainty. An overly simplified model does not always yield a valid result, yet a complicated model from a discretization method needs verification. The middle ground of an analysis that is neither a black box nor a flowed oversimplification helps validating trends and most importantly understand phenomena.

Manufacturers of motor casings are concerned of heat sources impinging on the external metallic shell causing rapid heating that may result in rupture of the casing and exposure of the solid fuel. These events happen in the millisecond regime and although in the past, this problem was addressed assuming a quasi-static condition, the rapid changes in properties may couple to wave propagation in the casing if a projectile strikes it simultaneously. Flexural stresses magnify and ultimately cause failure. This phenomenon cannot be captured from a quasi-static analysis.

The present work treats transient response of a thin cylinder with material inhomogeneity over a rectangular patch of the cylinder's surface. In this patch, modulus changes smoothly from E_0 to $E_0(1-\alpha)$ where $0 < \alpha < 1$. This simulates the response of a finite cylinder weakened locally by intense heating.

Section 2 treats the finite homogeneous cylinder. For simplicity and without loss of generality, the two ends of the cylinder are assumed simply supported. A simple solution in terms of trigonometric functions along the cylinder axis is then possible. For a thin cylinder, Koiter's (1960) equations excluding rotary inertia permit an infinite velocity of shear waves. This means that a shear pulse disperses almost instantaneously. This fault lies with the Kirchhoff hypothesis that plane sections remain plane and that wall cross section is always perpendicular to the mid-plane surface. A consistent set of plate equations was derived by Mindlin (1951) as a limiting case of the general three-dimensional theory of elasticity. These equations include rotary inertia and shear deformation, and limit shear waves to finite speed. Since these terms affect mostly the high frequency and high wave-number modes of flexural vibration, a simplification developed in Appendix A first takes up only inextensional equations of Mindlin. The correction is then applied to Koiter's equations as a factor multiplying rotary inertia.

Section 3 treats the cylinder with modulus inhomogeneity over a rectangular patch adopting the Galerkin method. Displacements are expanded in terms of trial functions taken as the orthogonal eigenfunctions of the homogeneous cylinder. The variational method minimizes the error committed in the equations of motion and eliminates spatial dependence yielding ordinary differential equations in the time dependent generalized coordinates of the expansion.

One limiting case is when the cylinder radius tends to infinity asymptotically producing a plate. Section 4 analyzes a disk with radial modulus inhomogeneity. Inhomogeneous properties are considered by

segmenting the disk into annular regions. Each segment has constant properties that differ from one segment to another. Segments are joined via transfer matrices relating stresses and displacements at the two boundaries of a segment. The stepwise discretization of modulus approaches the actual distribution as the number of segments increases. The other limiting case is when axial lengths of cylinder and patch tend to zero eliminating axial dependence. This limit leads to a ring with circumferential inhomogeneity. The ring is divided into arc segments joined by transfer matrices as in the case of the disk (Appendix C).

Section 5 discusses the effect of inhomogeneity on transient response of cylinder, disk and ring.

2. Homogeneous cylinder

For a homogeneous thin cylinder, Koiter's (1960) equations modified to include shear deformation are

$$\begin{aligned}
&\partial_x N_{xx} + 1/a\partial_\theta N_{x\theta} = \rho h \partial_{tt} u \\
&\partial_x N_{x\theta} + 1/a\partial_\theta N_{\theta\theta} - Q_\theta/a = \rho h \partial_{tt} \upsilon \\
&\partial_x Q_x + 1/a\partial_\theta Q_\theta + 1/a N_{\theta\theta} = \rho h \partial_{tt} w + p_w(x,\theta) f_w(t) \\
&Q_x = \partial_x M_{xx} + \frac{\rho h^3 \chi}{12}\partial_{xtt} w, \quad \chi = 1 + 2/\kappa(1-\nu) \\
&Q_\theta = 1/a\partial_\theta M_{\theta\theta} - 2\partial_x M_{x\theta} + \frac{\rho h^3 \chi}{12a}(\partial_{\theta tt} w + \partial_{tt}\upsilon)
\end{aligned} \tag{1}$$

(x, θ) are axial and circumferential coordinates, (a, h) are cylinder radius and thickness, (ρ, E_0, ν) are mass density, modulus and Poisson's ratio, t is time, (u, υ, w) are axial, circumferential and radial displacements, (N_{ij}, M_{ij}, Q_i) are extensional resultant, moment resultant and shear resultant, $\kappa = \pi^2/12$ is Mindlin's shear constant, and $p_w(x, \theta)$ and $f_w(t)$ are spatial and time dependence of the applied normal pressure. The shear deformation factor χ is derived in Appendix A. The constitutive law relating stress resultants to displacements gives

$$\begin{aligned}
&N_{xx} = N_0(\partial_x u + \nu(\partial_\theta \upsilon - w)/a) \\
&N_{\theta\theta} = N_0(\nu\partial_x u + (\partial_\theta \upsilon - w)/a) \\
&N_{x\theta} = (1-\nu)N_0(1/a\partial_\theta u + \partial_x \upsilon)/2 \\
&M_{xx} = -M_0(\partial_{xx} w + \nu(\partial_{\theta\theta} w + \partial_\theta \upsilon)/a^2) \\
&M_{\theta\theta} = -M_0(\nu\partial_{xx} w + (\partial_{\theta\theta} w + \partial_\theta \upsilon)/a^2) \\
&M_{x\theta} = (1-\nu)M_0(\partial_{x\theta} w + \partial_x \upsilon)/a \\
&N_0 = E_0 h/(1-\nu^2), \quad M_0 = E_0 h^3/12(1-\nu^2)
\end{aligned} \tag{2a}$$

Stresses are related to stress resultants by

$$\begin{aligned}
&\sigma_{xxe} = N_{xx}/h, \quad \sigma_{\theta\theta e} = N_{\theta\theta}/h \qquad \text{extensional} \\
&\sigma_{xxf} = 6M_{xx}/h^2, \quad \sigma_{\theta\theta f} = 6M_{\theta\theta}/h^2 \qquad \text{flexural} \\
&\tau_{xx} = 1.5Q_x/h, \quad \tau_{\theta\theta} = 1.5Q_\theta/h \qquad \text{shear}
\end{aligned} \tag{2b}$$

Substituting (2a) in (1) yields an eighth order system of partial differential equations in (u, υ, w):

$$\mathbf{Du} = \mathbf{p} \tag{3}$$

$$
\begin{aligned}
D_{11} &= N_0(\partial_{xx} + (1-\nu)/2a^2\partial_{\theta\theta}) - \rho h\partial_{tt}\\
D_{12} &= D_{21} = N_0(1+\nu)/2a\partial_{x\theta}\\
D_{13} &= D_{31} = -N_0\nu/a\partial_x\\
D_{22} &= N_0((1-\nu)/2\partial_{xx} + 1/a^2\partial_{\theta\theta}) + M_0/a^2(1/a^2\partial_{\theta\theta} + 2(1-\nu)\partial_{xx}) - (1+\chi\tilde{r}^2)\rho h\partial_{tt}\\
D_{23} &= D_{32} = -N_0/a^2\partial_\theta + M_0/a^2\partial_\theta(1/a^2\partial_{\theta\theta} + (2-\nu)\partial_{xx}) + \rho h\chi\tilde{r}^2\partial_{\theta tt}\\
D_{33} &= M_0\nabla^4 + N_0/a^2 + \rho h(1-\chi\tilde{r}^2a^2\nabla^2)\partial_{tt}\\
\nabla^2 &= \partial_{xx} + 1/a^2\partial_{\theta\theta}, \quad \nabla^4 = \nabla^2\nabla^2, \quad \tilde{r} = h/\sqrt{12}a
\end{aligned}
$$

D is a symmetric differential operator matrix, $\mathbf{u} = \{u, \upsilon, w\}^{\mathrm{T}}$ is the displacement vector and $\mathbf{p} = \{0, 0, p_w(x,\theta)f_w(t)\}^{\mathrm{T}}$ is vector of external tractions. Simply supported boundary conditions at $x = 0$ and $x = l$ are expressed as

$$\upsilon = w = N_{xx} = M_{xx} = 0 \tag{4}$$

l is cylinder length. For sinusoidal time dependence with radian frequency ω and for w motions symmetric about $\theta = 0$, the exact solution satisfying boundary condition (4) is

$$
\begin{aligned}
u(x,\theta;t) &= \sum_n \sum_m u_{nm}C_m(x)C_n(\theta)\mathrm{e}^{\mathrm{i}\omega t}, \quad s_m = m\pi/l\\
\upsilon(x,\theta;t) &= -\sum_n \sum_m \upsilon_{nm}S_m(x)S_n(\theta)\mathrm{e}^{\mathrm{i}\omega t}\\
w(x,\theta;t) &= \sum_n \sum_m w_{nm}S_m(x)C_n(\theta)\mathrm{e}^{\mathrm{i}\omega t}\\
S_m, C_m(x) &= \sin, \cos(s_m x), \quad S_n, C_n(\theta) = \sin, \cos(n\theta)
\end{aligned}
\tag{5}
$$

(n, m) are circumferential and axial wave numbers. The type of boundary condition does not affect wave propagation for times earlier than reflections from the boundaries. For other boundary conditions, relations (5) can be substituted with other functions that satisfy other boundary conditions. For the homogeneous cylinder, these functional forms are determined analytically since the eighth order differential operators (3) have constant coefficients yielding a solution in terms of exponentials:

$$
\begin{aligned}
u(x,\theta) &= \sum_n \sum_m \sum_{k=1}^{8} u_{knm}\mathrm{e}^{\lambda_{knm}x}C_n(\theta), \quad \upsilon(x,\theta) = \sum_n \sum_m \sum_{k=1}^{8} \upsilon_{knm}\mathrm{e}^{\lambda_{knm}x}S_n(\theta)\\
w(x,\theta) &= \sum_n \sum_m \sum_{k=1}^{8} w_{knm}\mathrm{e}^{\lambda_{knm}x}C_n(\theta)
\end{aligned}
\tag{5a}
$$

u_{knm}, υ_{knm}, w_{knm} are constant coefficients, and λ_{knm} are complex exponents that derive from the dispersion relation and are functions of ω, E, ρ, ν and h, a. The dispersion relation is obtained by substituting (5a) into (3) with periodic time dependence. The procedure with other boundary conditions is the same as that for classical simple supports, yet the analysis is more involved. Substituting (5) in (3) with $\mathbf{p} = \mathbf{0}$ produces a single set of homogeneous simultaneous equations for each (n, m) combination

$$(\mathbf{K_h} - \mathbf{M}\omega^2)_{nm}\bar{\mathbf{u}}_{nm} = \mathbf{0} \tag{6}$$

$\bar{\mathbf{u}}_{nm} = \{u_{mn}, \upsilon_{mn}, w_{mn}\}^{\mathrm{T}}$, $\mathbf{K_h}_{nm}$ is a symmetric stiffness matrix with coefficients

$$
\begin{aligned}
K_{h11,nm} &= \omega_0^2(\bar{s}_m^2 + (1-v)n^2/2)\\
K_{h12,nm} &= K_{h21,nm} = \omega_0^2(1+v)\bar{s}_m n/2\\
K_{h13,nm} &= K_{h31,nm} = \omega_0^2 v\bar{s}_m\\
K_{h22,nm} &= \omega_0^2((1-v)\bar{s}_m^2/2 + n^2 + \tilde{r}^2(2(1-v)\bar{s}_m^2 + n^2))\\
K_{h23,nm} &= K_{h32,nm} = \omega_0^2 n(1 + \tilde{r}^2((2-v)\bar{s}_m^2 + n^2))\\
K_{h33,nm} &= \omega_0^2(1 + \tilde{r}^2(\bar{s}_m^2 + n^2)^2)\\
\omega_0 &= \sqrt{E/\rho(1-v^2)}/a, \quad \bar{s}_m = as_m = m\pi a/l
\end{aligned}
\tag{7}
$$

$\mathbf{M}_{nm}$ is a symmetric mass matrix with coefficients

$$
\begin{aligned}
&M_{ij,nm} = 0 \ \ \forall ij \quad \text{except}\\
&M_{11,nm} = \rho h, M_{22,nm} = \rho h(1+\chi\tilde{r}^2), \quad M_{23,nm} = M_{32,nm} = \rho h n\chi\tilde{r}^2\\
&M_{33,nm} = \rho h(1 + \chi\tilde{r}^2(\bar{s}_m^2 + n^2))
\end{aligned}
\tag{8}
$$

A non-trivial solution to (6) yields the eigenvalue problem

$$\det|\mathbf{M}^{-1}\mathbf{K}_\mathbf{h} - \mathbf{I}\omega^2|_{nm} = 0 \tag{9a}$$

$\mathbf{I}$ is the unit matrix. Eq. (9a) determines the orthogonal eigenset

$$\{u_{nm}, \upsilon_{nm}, w_{nm}; \omega_{nm}\} \tag{9b}$$

For each (n, m) dyad, (9a) yields three distinct eigenfrequencies. The lowest frequency usually corresponds to a w dominant flexural mode while the intermediate and high frequencies correspond to u or υ dominant extensional modes.

Transient response to an external pressure pulse normal to the cylinder's surface is determined by the modal expansion

$$
\begin{aligned}
u(x,\theta;t) &= \sum_n \sum_m a_{nm}(t)u_{nm}C_m(x)C_n(\theta)\\
\upsilon(x,\theta;t) &= -\sum_n \sum_m a_{nm}(t)\upsilon_{nm}S_m(x)S_n(\theta)\\
w(x,\theta;t) &= \sum_n \sum_m a_{nm}(t)w_{nm}S_m(x)C_n(\theta)
\end{aligned}
\tag{10}
$$

$a_{nm}(t)$ is generalized coordinate of the (n, m) mode. Substituting (10) in (3) and enforcing orthogonality of the eigenfunctions produces a set of uncoupled ordinary differential equations in $a_{nm}(t)$,

$$
\begin{aligned}
&\ddot{a}_{nm}(t) + \omega_{nm}^2 a_{nm}(t) = -N_{fnm}f_w(t)/N_{nm}\\
&N_{fnm} = aw_{nm}\int_0^l \int_0^{2\pi} p_w(x,\theta)S_m(x)C_n(\theta)\,\mathrm{d}\theta\,\mathrm{d}x\\
&N_{nm} = \frac{1}{2}(1+\delta_{n0})\pi\rho hal[u_{nm}^2 + \upsilon_{nm}^2 + w_{nm}^2 + \tilde{r}^2\chi((\bar{s}_m w_{nm})^2 + (nw_{nm} + \upsilon_{nm})^2)]
\end{aligned}
\tag{11}
$$

$(\dot{\cdot})$ denotes time derivative and δ_{n0} is the Kronecker delta.

3. Inhomogeneous cylinder

Consider a cylinder with a modulus inhomogeneity in the form

$$\begin{aligned} &E(x,\theta) = E_0\varepsilon(x,\theta)\\ &\varepsilon(x,\theta) = \{1-\alpha[1-\operatorname{sech}(\beta(r+r_f))-\operatorname{sech}(\beta(r-r_f))]\}\Xi(x)\Theta(\theta)\\ &x_f - d_f \leqslant x \leqslant x_f + d_f, \quad -\theta_f \leqslant \theta \leqslant \theta_f \end{aligned} \tag{12a}$$

$$\begin{aligned} &r = ((x-x_f)^2 + (a\theta)^2)^{1/2}, \quad r_f = [(1-(a\theta_f/d_f)^2)(x-x_f)^2 + (a\theta_f)^2]^{1/2}\\ &\Xi(x) = H(x-x_f+d_f) - H(x-x_f-d_f)\\ &\Theta(\theta) = H(\theta+\theta_f) - H(\theta-\theta_f) \end{aligned} \tag{12b}$$

H is the Heaviside function. In (12), $E = E_0$ throughout the cylinder's surface except in a rectangular patch with side lengths $2d_f \times 2a\theta_f$ centered at $(x_f, 0)$ (see Fig. 1). For a square patch $d_f = a\theta_f$ and r_f lies on a circle with radius d_f while for a rectangular patch r_f lies on an ellipse with radii d_f and $a\theta_f$. This choice allows symmetry about the patch axes and a smooth transition from E_0 along the patch perimeter to $E_0(1-\alpha)$ at its center varying at a rate depending on β.

The equations of motion of the inhomogeneous cylinder are

$$\mathbf{Du} + \widetilde{\mathbf{D}}\mathbf{u} = \mathbf{p} \tag{13}$$

$\mathbf{D}$ is similar to the symmetric differential operator matrix $\mathbf{D}$ defined in (3) with the constants N_0 and M_0 replaced by the functions $N_0(x,\theta)$ and $M_0(x,\theta)$, and $\widetilde{\mathbf{D}}$ is a non-symmetric differential operator matrix listed below:

$$\begin{aligned} &\widetilde{D}_{11} = N_{0,x}\partial_x + (1-\nu)/2a^2 N_{0,\theta}\partial_\theta\\ &\widetilde{D}_{12} = N_{0,x}\nu/a\partial_\theta + (1-\nu)/2aN_{0,\theta}\partial_x\\ &\widetilde{D}_{13} = -N_{0,x}\nu/a \end{aligned} \tag{14a}$$

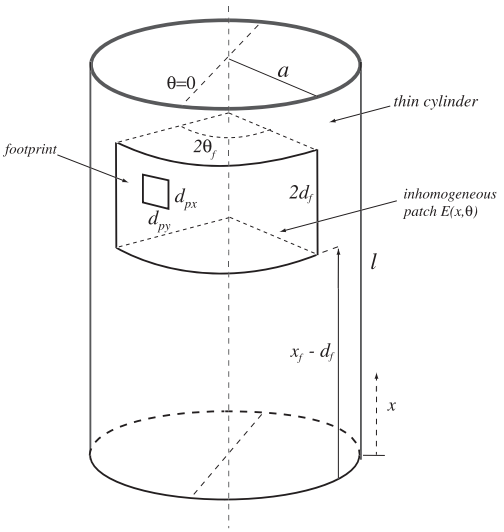

Fig. 1. Geometry of cylinder and inhomogeneous patch.

$$\begin{aligned}
\widetilde{D}_{21} &= N_{0,\theta}v/a\partial_x + (1-v)/2aN_{0,x}\partial_\theta \\
\widetilde{D}_{22} &= (1-v)(N_{0,x}/2 + 2M_{0,x}/a^2)\partial_x + (N_{0,\theta} + M_{0,\theta}/a^2)/a^2\partial_\theta \\
\widetilde{D}_{23} &= -N_{0,\theta}/a^2 + M_{0,\theta}/a^2(v\partial_{xx} + 1/a^2\partial_{\theta\theta}) + 2(1-v)M_{0,x}/a^2\partial_{x\theta}
\end{aligned} \tag{14b}$$

$$\begin{aligned}
\widetilde{D}_{31} &= 0 \\
\widetilde{D}_{32} &= 2(1-v)M_{0,x\theta}/a^2\partial_x + (vM_{0,xx} + M_{0,\theta\theta}/a^2)/a^2\partial_\theta \\
&\quad + 2M_{0,\theta}((1-v)\partial_{xx} + 1/a^2\partial_{\theta\theta})/a^2 + 2M_{0,x}/a^2\partial_{x\theta} \\
\widetilde{D}_{33} &= (M_{0,xx} + vM_{0,\theta\theta}/a^2)\partial_{xx} + (vM_{0,xx} + M_{0,\theta\theta}/a^2)/a^2\partial_{\theta\theta} \\
&\quad + 2(1-v)M_{0,x\theta}/a^2\partial_{x\theta} + 2M_{0,x}\partial_{xxx} + 2M_{0,\theta}/a^2\partial_{xx\theta} \\
&\quad + 2M_{0,x}/a^2\partial_{x\theta\theta} + 2M_{0,\theta}/a^4\partial_{\theta\theta\theta}
\end{aligned} \tag{14c}$$

In (14) subscripts x and θ following a comma stand for partial derivatives with respect to x and θ respectively.

The Galerkin method is utilized to solve (13). Eigenfunctions of the homogeneous cylinder are taken as trial functions. Substituting (10) in (13) yields

$$\begin{aligned}
&\sum_j \sum_k \{N_0[(s_j^2 + (1-v)(k/a)^2/2)u_{kj} + (1+v)s_jk/2av_{kj} + vs_j/aw_{kj}]C_j(x)C_k(\theta) \\
&\quad + N_{0,\theta}(1-v)/2a(k/au_{kj} + s_jv_{kj})C_j(x)S_k(\theta) + N_{0,x}(s_ju_{kj} + vk/av_{kj} + v/aw_{kj})S_j(x)C_k(\theta)\}a_{kj}(t) \\
&\quad + \rho h \sum_k \sum_j u_{kj}C_j(x)C_k(\theta)\ddot{a}_{kj}(t) = 0
\end{aligned} \tag{15a}$$

$$\begin{aligned}
&\sum_k \sum_j \{[N_0(1+v)s_j(k/2a)u_{kj} + (N_0((1-v)s_j^2/2 + (k/a)^2) + M_0(2(1-v)s_j^2 + (k/a)^2)/a^2)v_{kj} \\
&\quad + k(M_0((2-v)s_j^2 + (k/a)^2) + N_0)/a^2w_{kj}]S_j(x)S_k(\theta) - [N_{0,x}(1-v)(k/2a)u_{kj} \\
&\quad + (1-v)s_j(N_{0,x}/2 + 2M_{0,x}/a^2)v_{kj} + 2M_{0,x}(1-v)s_jk/a^2w_{kj}]C_j(x)S_k(\theta) - [N_{0,\theta}vs_j/au_{kj} \\
&\quad + k(N_{0,\theta} + M_{0,\theta}/a^2)/a^2v_{kj} + (N_{0,\theta}/a^2 + M_{0,\theta}(vs_j^2 + (k/a)^2)/a^4)w_{kj}]S_j(x)C_k(\theta)\}a_{nm}(t) \\
&\quad + \rho h \sum_k \sum_j [(1 + \tilde{r}^2\chi)v_{kj} - \tilde{r}^2\chi kw_{kj}]S_j(x)S_k(\theta)\ddot{a}_{kj}(t) = 0
\end{aligned} \tag{15b}$$

$$\begin{aligned}
&\sum_k \sum_j \{[N_0vs_j/au_{kj} + (M_0(s_j^4 + (k/a)^4 + 2(s_jn/a)^2) + N_0/a^2 - M_{0,xx}(s_j^2 + v(k/a)^2) \\
&\quad - M_{0,\theta\theta}(vs_j^2 + (k/a)^2)/a^2)w_{kj} + k(N_0 + M_0((2-v)s_j^2 + (k/a)^2) - M_{0,xx}v - M_{0,\theta\theta}/a^2)/a^2v_{kj}]S_j(x)C_k(\theta) \\
&\quad - 2M_{0,x\theta}[(1-v)s_j(v_{kj} + kw_{kj})/a^2]C_j(x)S_k(\theta) - 2M_{0,x}s_j[kv_{kj}/a^2 + (s_j^2 + (k/a)^2)w_{kj}]C_j(x)C_k(\theta) \\
&\quad + M_{0,\theta}[2((1-v)s_j^2 + (k/a)^2)v_{kj} + k(s_j^2 + (k/a)^2)w_{kj}]/a^2S_j(x)S_k(\theta)\}a_{kj}(t) \\
&\quad + \rho h \sum_k \sum_j [-k\tilde{r}^2\chi v_{kj} + (1 + \tilde{r}^2\chi((as_j)^2 + k^2))w_{kj}]S_j(x)C_j(\theta)\ddot{a}_{kj}(t) = p_w(x,\theta)f_w(t)
\end{aligned} \tag{15c}$$

where the following notation was used:

$$S_j, C_j(x) = \sin, \cos(s_jx), \quad S_k, C_k(\theta) = \sin, \cos(k\theta)$$

Multiplying (15a) by $C_m(x)C_n(\theta)u_{nm}$, (15b) by $S_m(x)S_n(\theta)\upsilon_{nm}$, and (15c) by $S_m(x)C_n(\theta)w_{nm}$, integrating over the cylinder surface, then adding the three equations yields a system of $3m_xn_\theta$ coupled ordinary differential equations in the generalized coordinates a_{nm},

$$\begin{aligned}
&\mathbf{K}_c\mathbf{a}+\mathbf{M}\ddot{\mathbf{a}}=\mathbf{f}f_w(t) \qquad (16)\\
&K_{cmn,jk}=\sum_{i_1=1}^{3}\sum_{i_2=1}^{3}C_{mn,jk}^{(i_1i_2)}+C_{mn,jk}^{(34)};\quad 1\leqslant m\leqslant m_x, 0\leqslant n\leqslant n_\theta\\
&M_{mn,jk}=\frac{1}{2}(1+\delta_{n0})\delta_{mj}\delta_{nk}\pi\rho hal[u_{nm}^2+\upsilon_{nm}^2+w_{nm}^2+\tilde{r}^2\chi((as_m)^2w_{nm}^2+(nw_{nm}+\upsilon_{nm})^2)]\\
&\mathbf{f}=\{0,0,N_{fnm}\}^{\mathrm{T}}
\end{aligned}$$

$\mathbf{a}=\{a_{nm}\}^{\mathrm{T}}$ is the vector of generalized coordinates and N_{fnm} is generalized force defined by (11). Let m_x and n_θ be the truncated number of terms in the m and n series of the constituent modes in (10), then the number of equations in (16) is $3m_xn_\theta$ which is triple the number of dyads (m, n), to include the three distinct eigenfunctions $(u_{nm}, \upsilon_{nm}, w_{nm})_{1,2,3}$ for each dyad corresponding to the w_{nm}-dominant flexural motion, the u_{nm}-dominant and the υ_{nm}-dominant extensional motion. Coefficients $C_{mn,jk}^{(i_1i_2)}$ of the coupled stiffness matrix $\mathbf{K}_c$ are defined in Appendix B and coefficients of the diagonal mass matrix $\mathbf{M}$ are identical to N_{nm} in (11).

To diagonalize (16), form the coupled eigenproblem

$$[\mathbf{M}^{-1}\mathbf{K}_c-\mathbf{I}\omega_c^2]\mathbf{a}=\mathbf{0} \qquad (17)$$

The eigenproblem (17) yields the orthogonal eigenset $\{\Phi_{cl}(x,\theta);\omega_{cl}\}$ where $\Phi_{cl}(x,\theta)$ is the lth eigenvector coupling the constituent modes $\{u_{nm}, \upsilon_{nm}, w_{nm}\}^{\mathrm{T}}$ by the coupling coefficients $a_{nm,l}$, and ω_{cl} are the corresponding coupled eigenfrequencies. Expand the coupled displacement vector $\mathbf{u}_c=\{u_c,\upsilon_c,w_c\}^{\mathrm{T}}$ in terms of $\Phi_{cl}(x,\theta)$,

$$\begin{aligned}
&\mathbf{u}_c(x,\theta;t)=\sum_l c_l(t)\Phi_{cl}(x,\theta)\\
&\Phi_{cl}(x,\theta)\equiv\{u_{cl},\upsilon_{cl},w_{cl}\}^{\mathrm{T}}=\sum_{n=0}\sum_{m=1}a_{nm,l}\mathbf{u}_{nm}(x,\theta)
\end{aligned} \qquad (18a)$$

$$\begin{aligned}
&u_c(x,\theta;t)=\sum_l c_l(t)u_{cl}(x,\theta), u_{cl}(x,\theta)=\sum_{n=0}\sum_{m=1}a_{nm,l}u_{nm}C_m(x)C_n(\theta)\\
&\upsilon_c(x,\theta;t)=\sum_l c_l(t)\upsilon_{cl}(x,\theta), \upsilon_{cl}(x,\theta)=\sum_{n=1}\sum_{m=1}a_{nm,l}\upsilon_{nm}S_m(x)S_n(\theta)\\
&w_c(x,\theta;t)=\sum_l c_l(t)w_{cl}(x,\theta), w_{cl}(x,\theta)=\sum_{n=0}\sum_{m=1}a_{nm,l}w_{nm}S_m(x)C_n(\theta)
\end{aligned} \qquad (18b)$$

$c_l(t)$ is generalized coordinate of the lth coupled eigenfunction and $\mathbf{u}_{nm}$ is displacement vector of the (m, n)th constituent mode. Substituting (18) in (13) and enforcing orthogonality of the $\{u_{cl}, \upsilon_{cl}, w_{cl}\}$ set yields uncoupled equations in $c_l(t)$

$$\ddot{c}_l(t)+\omega_{cl}^2c_l(t)=N_{cfl}f_w(t) \qquad (19)$$

$$N_{cfl}=4a/N_{cll}\int_{x_f}^{x_f+d_f}\int_0^{\theta_f}p_w(x,\theta)w_{cl}\,\mathrm{d}\theta\,\mathrm{d}x$$

$$\begin{aligned}
N_{cll}&=a\int_0^l\int_0^{2\pi}(u_{cl}^2+\upsilon_{cl}^2+w_{cl}^2+\tilde{r}^2\chi(\upsilon_{cl}^2-a^2w_{cl}\nabla^2w_{cl}-\upsilon_{cl}\partial_\theta w_{cl}+w_{cl}\partial_\theta\upsilon_{cl}))\,\mathrm{d}\theta\,\mathrm{d}x\\
&=\pi\rho hal/2\sum_{n=0}\sum_{m=1}(1+\delta_{n0})a_{nm,l}^2[u_{nm}^2+\upsilon_{nm}^2+w_{nm}^2+\tilde{r}^2\chi((\bar{s}_mw_{nm})^2+(nw_{nm}+\upsilon_{nm})^2)]
\end{aligned}$$

Eq. (19) admits the solution

$$c_l(t) = -\frac{N_{cfl}}{\omega_{ci}} \int_0^t \sin \omega_{cl}(t-\tau) f_w(\tau)\, \mathrm{d}\tau \tag{20}$$

If $f_w(t)$ is piecewise linear with n_s conjoined segments

$$\begin{aligned} f_w(t) &= \sum_{j=1}^{n_s} (\zeta_j + \eta_j(t-t_j))[H(t-t_j) - H(t-t_{j+1})] \\ \eta_j &= (f_w(t_{j+1}) - f_w(t_j))/(t_{j+1}-t_j), \zeta_j = f_w(t_j), t_1 = f_w(t_1) = 0 \end{aligned} \tag{21}$$

Eq. (20) can then be integrated analytically.

4. Inhomogeneous disk

In the limit as the cylinder's mean radius approaches infinity, the cylinder's surface approaches a plate. Furthermore, prior to reflections from the boundary, the region neighboring the excitation can be approximated by a finite disk with diameter equal to cylinder length forced by an axially symmetric pressure acting over a circular footprint. An inhomogeneous modulus is considered by segmenting the disk into annular regions. Each segment is homogeneous with constant properties that differ from one segment to another. As the number of segments increases, the stepwise approximation of properties approaches the continuous distribution.

Mindlin's axisymmetric equations for a disk are

$$[(\nabla^2 - 1/c_\varepsilon^2 \partial_{tt})(\nabla^2 - 1/c_s^2 \partial_{tt}) + 12/(c_\varepsilon h)^2 \partial_{tt}]w = [1/D - (\nabla^2 - 1/c_\varepsilon^2 \partial_{tt})/\kappa G h]p \tag{22a}$$

$$[D\nabla^2 - \rho h^3/12 \partial_{tt}]\partial_r \psi = \rho h \partial_{tt} w - p \tag{22b}$$

$$\begin{aligned} &\nabla^2 \equiv \partial_{rr} + 1/r\partial_r \\ &c_\varepsilon^2 = E_0/\rho(1-\nu^2), \quad c_s^2 = \kappa G/\rho, \quad G = E_0/2(1+\nu), \quad D = E_0 h^3/12(1-\nu^2) \end{aligned}$$

where (w, ψ) are axial displacement and rotation, p is applied pressure, (E_0, G, ν, ρ) are Young's modulus, shear modulus, Poisson's ratio and mass density, (h, r_d) are disk thickness and radius, and κ is shear constant. Assume that $E(r)$ follows the axisymmetric profile

$$E(r) = E_0\{1 - \alpha[1 - \operatorname{sech}(\beta(r + d_f)) - \operatorname{sech}(\beta(r - d_f))]\}; \quad 0 \leqslant r \leqslant d_f \tag{22c}$$

consistent with that of the cylinder in Eq. (12). Divide the disk into m_s annular segments $r_{sj} \leqslant r \leqslant r_{sj+1}$, $1 \leqslant j \leqslant m_s + 1$ enclosing the central disk $0 \leqslant r \leqslant r_{s1}$. Discretize (22c) into steps with modulus $E_f, E_1, \ldots, E_j, \ldots, E_{m_s}$ where $E_f \simeq E_0(1-\alpha_f)$ applies to the central portion and E_j applies to segment $r_{sj} \leqslant r \leqslant r_{sj+1}$. For frequency response outside the central disk, the solution to the jth segment is

$$\begin{aligned} w_j(r) &= C_{1j} J_0(k_{1j} r) + C_{2j} Y_0(k_{1j} r) + C_{3j} J_0(k_{2j} r) + C_{4j} Y_0(k_{2j} r) \\ \psi_j(r) &= \delta_{1j}(C_{1j} J_0'(k_{1j} r) + C_{2j} Y_0'(k_{1j} r)) + \delta_{2j}(C_{3j} J_0'(k_{2j} r) + C_{4j} Y_0'(k_{2j} r)) \\ \delta_{lj} &= (-k_{lj}^2 + \omega^2/c_{sj}^2)/k_{lj}, \quad l = 1, 2 \end{aligned} \tag{23}$$

$k_{1,2j}$ are roots of the dispersion relation

$$(k_j^2 - 1/c_{\varepsilon j}^2 \omega^2)(k_j^2 - 1/c_{sj}^2 \omega^2) - 12/(c_{\varepsilon j} h)^2 \omega^2 = 0 \tag{24}$$

For the central disk, the solution bounded at the origin is

$$\begin{aligned} w_0(r) &= C_{10}J_0(k_{10}r) + C_{30}J_0(k_{20}r) \\ \psi_0(r) &= \delta_{10}C_{10}J_0'(k_{10}r) + \delta_{20}C_{30}J_0'(k_{20}r) \end{aligned} \tag{25}$$

Moment and shear resultants are

$$M_{rr} = D(\partial_r\psi + \nu\psi/r), \quad Q_{rr} = \kappa Gh(\partial_r w + \psi) \tag{26}$$

Substituting (25) in (26) and defining $\mathbf{f}_0 = \{Q_{rr}, M_{rr}\}_0^{\mathrm{T}}, \mathbf{g}_0 = \{w, \psi\}_0^{\mathrm{T}}$ yields

$$\mathbf{f}_0 = \mathbf{B}_{\mathbf{f}0}\mathbf{C}_0, \quad \mathbf{g}_0 = \mathbf{B}_{\mathbf{g}0}\mathbf{C}_0 \tag{27}$$

$\mathbf{C}_0 = \{C_{10}, C_{30}\}^{\mathrm{T}}$, $\mathbf{B}_{\mathbf{f}0}$ and $\mathbf{B}_{\mathbf{g}0}$ are 2×2 matrices with coefficients involving the radial functions and their derivatives in (25) and (26). Evaluating (27) at $r = r_{s1}$ and eliminating $\mathbf{C}_0$ yields an impedance relation

$$\mathbf{f}_0 = \mathbf{B}_{\mathbf{g}0}^{-1}(r_{s1})\mathbf{B}_{\mathbf{f}0}(r_{s1})\mathbf{g}_0 \equiv \mathbf{Z}_0\mathbf{g}_0 \tag{28}$$

Substituting (23) in (26) and defining $\mathbf{f}_j = \{Q_{rr}, M_{rr}\}_j^{\mathrm{T}}, \mathbf{g}_j = \{w, \psi\}_j^{\mathrm{T}}$ yields

$$\mathbf{f}_j = \mathbf{B}_{\mathbf{f}\,j}\mathbf{C}_j, \quad \mathbf{g}_j = \mathbf{B}_{\mathbf{g}\,j}\mathbf{C}_j \tag{29}$$

$\mathbf{C}_j = \{C_{1j}, C_{2j}, C_{3j}, C_{4j}\}^{\mathrm{T}}$, $\mathbf{B}_{\mathbf{f}j}$ and $\mathbf{B}_{\mathbf{g}j}$ are 2×4 matrices with coefficients involving the radial functions and their derivatives in (23) and (26). Defining the state vector at an interface as $\mathbf{S}_j = \{\mathbf{f}_j, \mathbf{g}_j\}^{\mathrm{T}}$ then evaluating (29) at the two boundaries of segment j then finally eliminating $\mathbf{C}_j$ determines the transfer matrix of a segment relating $\mathbf{S}_j(r_{sj})$ to $\mathbf{S}_j(r_{sj+1})$

$$\begin{aligned} &\mathbf{S}_j(r_{sj+1}) = \mathbf{T}_{j,j+1}\mathbf{S}_j(r_{sj}) \equiv \mathbf{B}_{\mathbf{s}\,j}^{-1}(r_{sj})\mathbf{B}_{\mathbf{s}\,j}(r_{sj+1})\mathbf{S}_j(r_{sj}) \\ &\mathbf{B}_{\mathbf{s}\,j} = \begin{bmatrix} \mathbf{B}_{\mathbf{f}\,j} \\ \mathbf{B}_{\mathbf{g}\,j} \end{bmatrix} \end{aligned} \tag{30}$$

Enforcing continuity of $\mathbf{f}_j$ and $\mathbf{g}_j$ at interfaces of segments and the impedance relation (28) at the first interface produces a set of $m_s + 1$ tri-diagonal block matrices in the interface state vectors $\mathbf{S}_j$. For the case of 3 annular segments and a clamped boundary, the tri-diagonal block system takes the form

$$\begin{bmatrix} \mathbf{I} & -\mathbf{Z}_0 & \mathbf{0} & \mathbf{0} & & & & \\ \mathbf{t}_{11,1} & \mathbf{t}_{12,1} & -\mathbf{I} & \mathbf{0} & & & & \\ \mathbf{t}_{21,1} & \mathbf{t}_{22,1} & \mathbf{0} & -\mathbf{I} & \mathbf{0} & \mathbf{0} & & \\ \mathbf{0} & \mathbf{0} & \mathbf{t}_{11,2} & \mathbf{t}_{12,2} & -\mathbf{I} & \mathbf{0} & & \\ & & \mathbf{t}_{21,2} & \mathbf{t}_{22,2} & \mathbf{0} & -\mathbf{I} & \mathbf{0} & \mathbf{0} \\ & & \mathbf{0} & \mathbf{0} & \mathbf{t}_{11,3} & \mathbf{t}_{12,3} & -\mathbf{I} & \mathbf{0} \\ & & & & \mathbf{t}_{21,3} & \mathbf{t}_{22,3} & \mathbf{0} & -\mathbf{I} \\ & & & & \mathbf{0} & \mathbf{0} & \mathbf{0} & \mathbf{I} \end{bmatrix} \begin{Bmatrix} \mathbf{f}_1 \\ \mathbf{g}_1 \\ \mathbf{f}_2 \\ \mathbf{g}_2 \\ \mathbf{f}_3 \\ \mathbf{g}_3 \\ \mathbf{f}_4 \\ \mathbf{g}_4 \end{Bmatrix} = \begin{Bmatrix} \mathbf{p} \\ \mathbf{0} \\ \mathbf{0} \\ \mathbf{0} \\ \mathbf{0} \\ \mathbf{0} \\ \mathbf{0} \\ \mathbf{0} \end{Bmatrix} \tag{31}$$

$$\begin{bmatrix} \mathbf{t}_{11,j} & \mathbf{t}_{12,j} \\ \mathbf{t}_{21,j} & \mathbf{t}_{22,j} \end{bmatrix} = \mathbf{T}_{j,j+1}$$

$\mathbf{I}$ and $\mathbf{0}$ are 2×2 unit and null matrices. Re-write Eq. (31) as

$$\mathbf{T}_G\mathbf{S}_G = \mathbf{P} \tag{32}$$

$\mathbf{T}_G$ is the global transfer matrix (31) and $\mathbf{S}_G = \{\mathbf{S}_1, \mathbf{S}_2, \ldots, \mathbf{S}_j, \ldots, \mathbf{S}_{m_s+1}\}^{\mathrm{T}}$ is the global state vector formed of the ensemble of all interface state vectors. The homogeneous form of (32) yields the eigenvalue problem

$$\det|\mathbf{T}_G| = 0 \tag{33}$$

and the eigenset $\{\mathbf{\Phi}_k, \omega_k\}$ with $\mathbf{\Phi}_k = \{\boldsymbol{\phi}_{1,k}, \boldsymbol{\phi}_{2,k}, \ldots, \boldsymbol{\phi}_{j,k}, \ldots, \boldsymbol{\phi}_{m_s,k}\}^{\mathrm{T}}$, $\boldsymbol{\phi}_{j,k} = \{\varphi_j, \eta_j\}_k$ being the kth displacement eigenvector of the jth segment.

Transient response is determined by expanding the global displacement vector $\mathbf{G}_G = \{\mathbf{g}_1, \mathbf{g}_2, \ldots, \mathbf{g}_j, \ldots, \mathbf{g}_{m_s}\}^{\mathrm{T}}$ in its eigenfunctions

$$\mathbf{G}_G = \sum_k a_k(t)\mathbf{\Phi}_k(r) \tag{34}$$

Substituting (34) in (22) and enforcing orthogonality of the eigenfunctions produces uncoupled ordinary differential equations in the generalized coordinates $a_k(t)$

$$\begin{aligned} &\ddot{a}_k(t) + \omega_k^2 a_k(t) = -N_{fk}/N_{kk} \\ &N_{fk} = \langle \mathbf{\Phi}_k|\mathbf{p}\rangle, N_{kk} = \rho h\langle \mathbf{\Phi}_k|\mathbf{\Phi}_k\rangle \end{aligned} \tag{35}$$

ω_k is the kth mode eigenfrequency.

5. Results

Consider a thin steel cylinder with 12.7 cm (=5 in.) mean radius, 50.8 cm (=20 in.) long and 1.27 cm (=0.5 in.) plate thickness, and material properties $E_0 = 2.1 \times 10^{12}$ dyn/cm^2 ($=30 \times 10^6$ psi), $\rho = 8$ g/cm^3 ($=7.5 \times 10^{-4}$ lbs^2/in.^{4}), $v = 0.3$. Modulus inhomogeneity is in the form of Eq. (12a) with $\alpha = 0.8$, $\beta = 5$, $d_f = 7.6$ cm (=3 in.) and $a\theta_f = 7.6$ cm (=3 in.). Coordinates of a point on the cylinder surface are denoted by (x_c, y) where $x_c = x - x_f$ is the axial coordinate relative to center of impact and $y = a\theta$ is an intrinsic length along the circumference (see Fig. 1).

The external excitation is a trapezoidal pressure pulse of unit intensity with 2 μs rise and fall times, and a 48 μs plateau, uniformly distributed over a square footprint with side $d_{px} = d_{py} = 2.25$ cm (=0.886 in.) centered at $(x_c, \theta) = (0, 0)$. This square footprint matches the area of a circular footprint with radius $r_p = 1.27$ cm (= 0.5 in.). Location of footprint center imposes axial symmetry about $x_c = 0$ so that only axial functions with odd m are included. This way, a total 1840 modes are included in the modal expansion.

Fig. 2(a)–(c) plots resonance spectra versus n with odd m as parameter for the low, intermediate and high frequency modes (ω_{L}, ω_{I}, ω_{H}) in the range $0 \leqslant n \leqslant 30$ and $1 \leqslant m \leqslant 39$. For this interval of wave numbers, resonances lie in the range 0.5 KHz $< \omega_{\mathrm{L}} <$ 150 KHz, 1 KHz $< \omega_{\mathrm{I}} <$ 170 KHz and 3 KHz $< \omega_{\mathrm{L}} <$ 280 KHz. For $n = 0$, only ω_{L} and ω_{I} are included while ω_{H} is dropped as it corresponds to torsion modes that do not couple in response to pure radial excitation.

Fig. 3 plots histories of the homogeneous cylinder at axial stations $x_c/r_p = 0, 3, 6, 9$ along $\theta = 0$. Radial displacement w peaks at $t = 50$ μs corresponding to the time interval of the forcing pulse Δt_f (Fig. 3(a)). w then falls to a plateau at 150 μs. At stations remote from the center of impact, w rises after a delay corresponding to travel time of flexural waves from the footprint to that station with the phase velocity $c_p < \sqrt{\kappa/2(1+v)}c_e, c_e = \sqrt{E/\rho}$ being the extensional speed. Axial displacement u is an order of magnitude smaller than w and propagates with c_e (Fig. 3(a2)). At $x_c = 0$, flexural stresses σ_{xxf} and $\sigma_{\theta\theta f}$ (Fig. 3(b1) and (c1)) rise sharply following impact peaking at $t = \Delta t_f$ with magnitude 3 times applied pressure then fall smoothly to zero. Remote from impact, magnitude of peak flexural stress does not exceed applied pressure and shows a time delay corresponding to c_e since u and v couple to flexural stresses. Extensional stress σ_{xxe} (Fig. 3(b2)) is an order of magnitude smaller than σ_{xxf} while $\sigma_{\theta\theta e} \approx 3\sigma_{xxe}$ (Fig. 3(c2)), and both propagate with c_e.

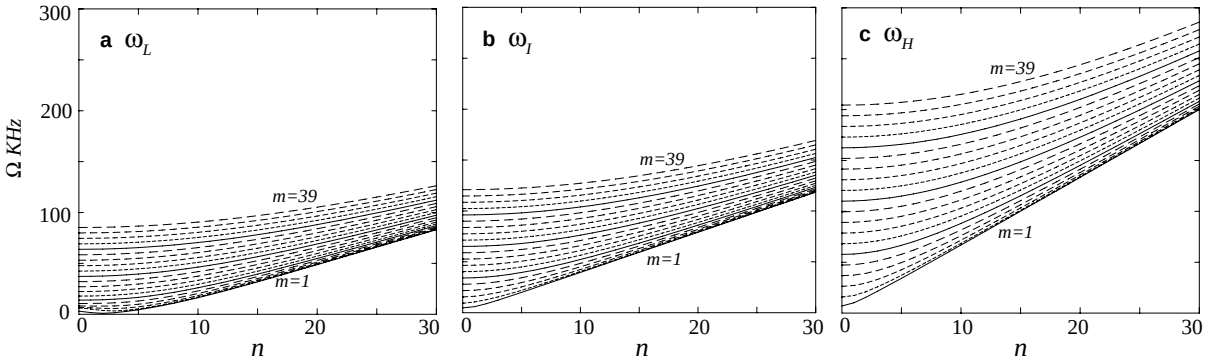

Fig. 2. Frequency spectra of homogeneous cylinder: (a) low frequencies ω_{L}, (b) intermediate frequencies ω_{I}, (c) high frequencies ω_{H}.

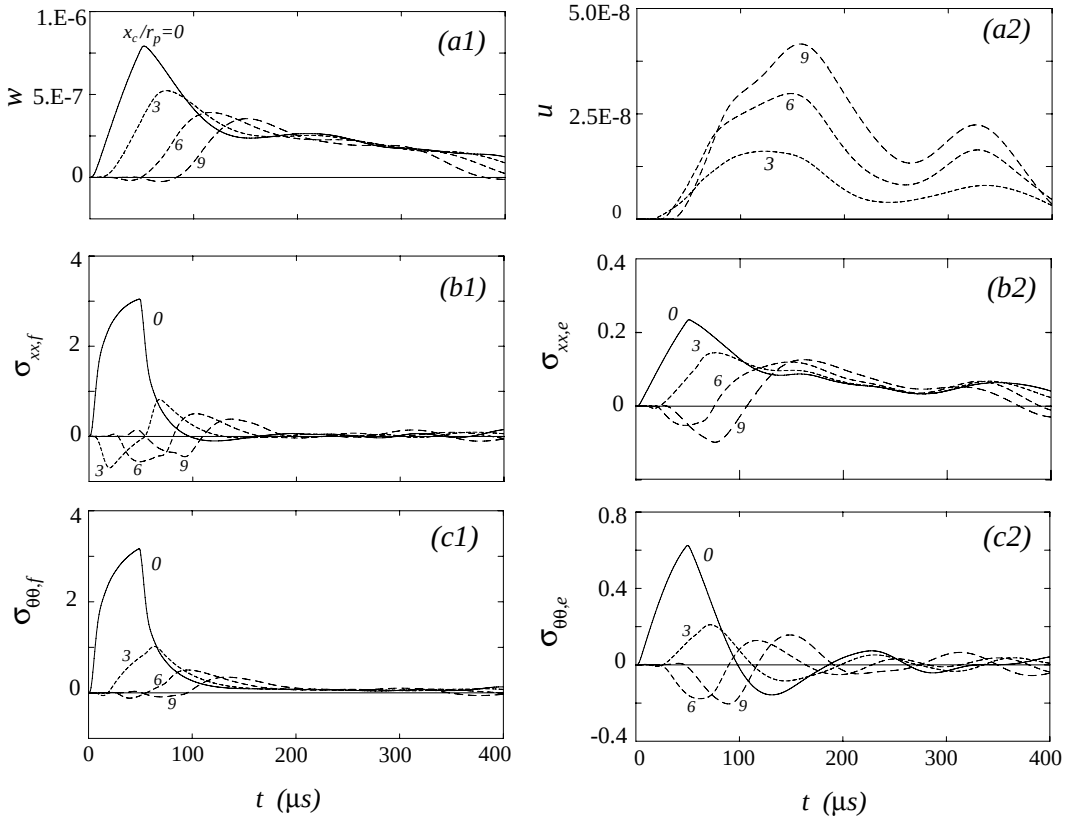

Fig. 3. Histories of homogeneous cylinder at $y = 0$: —— $x_c/r_p = 0$, ---- 3, –– 6, —— 9.

Fig. 4 plots histories of the homogeneous cylinder at y stations $y/r_p = 0, 3, 6, 9$ along $x_c = 0$. Comparing dependent variables in Fig. 4 with the corresponding ones in Fig. 3 reveals that remote from impact, response is not axially symmetric about the center of impact. The magnitude of circumferential displacement υ (Fig. 4(a2)) is twice that of u.

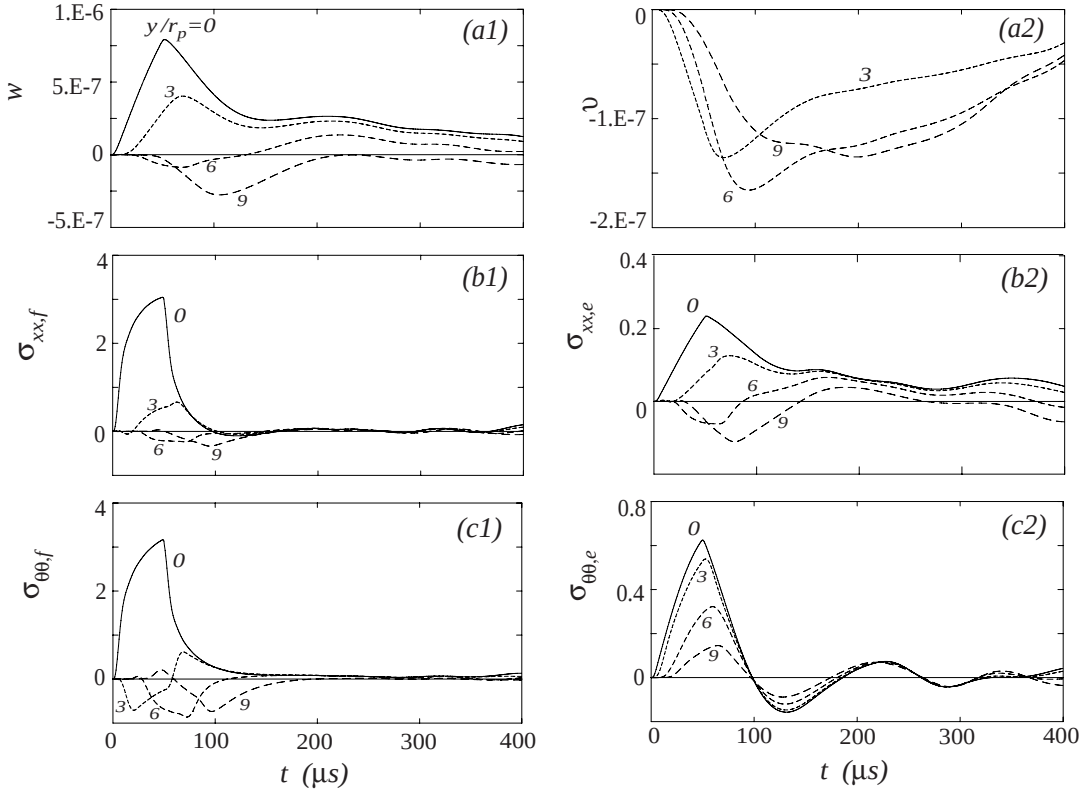

Fig. 4. Histories of homogeneous cylinder at $x_c/r_p = 0$: —— $y/r_p = 0$, ---- 3, ––– 6, —— 9.

Before discussing histories of the inhomogeneous cylinder, important features of the coupled modes are outlined. The basic difference in modal properties of homogeneous and inhomogeneous cylinders concerns three items: (i) eigenfrequencies, (ii) eigenfunctions, and (iii) normalized modal displacements. Examining modal results from the disk and ring models aids in the understanding of modal properties.

Fig. 5(a) plots $d = 100(\omega_h - \omega_c)/\omega_h$ where ω_h and ω_c are eigenfrequencies of the homogeneous and inhomogeneous cylinders sorted in ascending order. Both sets include ω_L,ω_I and ω_H. d starts at 20% for the fundamental then falls to 10% for $\Omega < 25$ KHz except at a few isolated frequencies. For $\Omega > 25$ KHz, d falls to very small values. Consequently, eigenfrequencies of the inhomogeneous cylinder are close to those of the homogeneous cylinder except at isolated frequencies. In contrast, the average d of disk and ring is approximately constant at 20%. This value approximately equals θ_f/π where θ_f is half arc angle of the inhomogeneous segment.

Fig. 6 plots the modal dependent variables with w_{max} normalized to unity of a typical coupled mode at $\Omega = 3.01$ KHz. Fig. 6(a1)–(d1) plot variables along x at $\theta = 0$ while Fig. 6(a2)–(d2) plot variables along θ at $x_c = 0$. Except for u and υ which are comparable to w, all variables are relatively small within the inhomogeneous patch

$$-d_f \leqslant x_c \leqslant d_f \quad , 0 \leqslant \theta \leqslant \theta_f, \quad 2\pi - \theta_f \leqslant \theta \leqslant 2\pi$$

Fig. 7 plots modal variables for a mode for a neighboring mode at $\Omega = 3.39$ KHz. Within the patch, all variables are relatively larger than in the 3.01 KHz mode while u and υ are still comparable to w. For most modes, w in the patch is smaller than w_{max} and u, υ are unusually large compared to corresponding modes

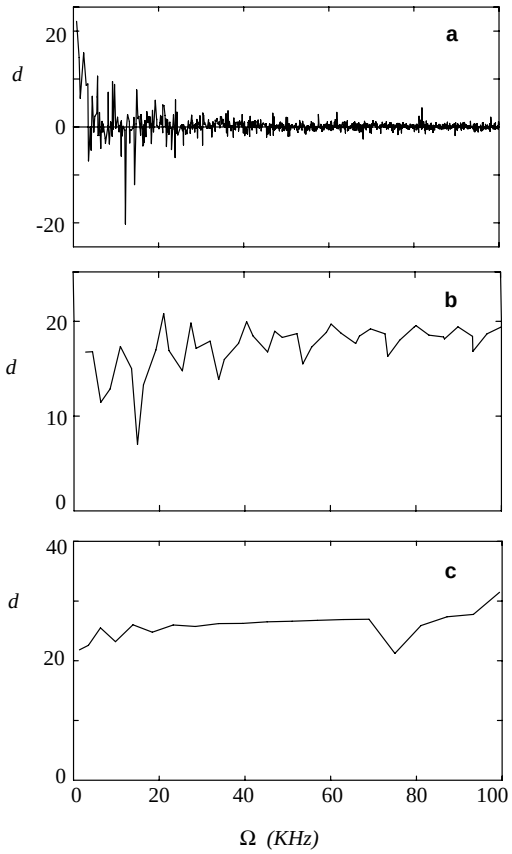

Fig. 5. Percent difference in Ω from inhomogeneity—$\alpha = 0.8$, $\beta = 5$: (a) cylinder $a\theta_f = d_f = 7.62$ cm, (b) ring $a\theta_f = 7.62$ cm, (c) disk $r_f = 7.62$ cm.

of the homogeneous cylinder. One way to identify the dominant (m, n) dyad of a coupled mode is by choosing the (m, n) of the constituent mode with largest $|a_{mn,i}|$.

Fig. 8 plots normalized average v_{avr} and w_{avr} versus mode number. For each mode v_{avr} is the ratio of v_{max} within the patch and w_{max} which is normalized to unity. The same applies to w_{avr}. Since the actual distribution of v_{avr} and w_{avr} changes substantially from mode to mode, it is convenient to smooth data by "Fast Fourier transform Filtering" with a 10-point sampling window. The result is a smooth average shown in Fig. 8. For the inhomogeneous cylinder, w_{avr} (Fig. 8(a1)) is almost constant at 0.5 with fluctuations of ± 0.1. This means that for most modes, w_{avr} in the patch is predominantly smaller than that outside the patch. v_{avr} (Fig. 8(b1)) rises with mode number peaking near mode 1000 where $\omega_{I,1}$ lies. It then falls sharply to values comparable with those at low ω_L. For the ring (Fig. 8(a2)), w_{avr} is close to unity at low frequencies and diminishes up to the 40th mode then rises again near the fundamental extensional frequency $\omega_{H,1}$ and maintains a value of approximately 0.75. In the patch, the ring's w_{avr} is larger than the cylinder's with the same parameters (α, β, d_f). The ring's v_{avr} (Fig. 8(b2)) resembles that of the cylinder without the falloff following $\omega_{H,1}$ since for the ring the u-dominant modes do not exist. The cylinder's u_{avr} closely follows v_{avr} in shape and magnitude. This suggests that inhomogeneity may magnify extensional stresses in the cylinder.

Fig. 9 plots histories of the inhomogeneous cylinder at $x_c/r_p = 0, 3, 6, 9$ along $\theta = 0$. Within the patch, comparing the same variables in Figs. 9 and 3 reveals that the inhomogeneity reduces w by a factor of 2

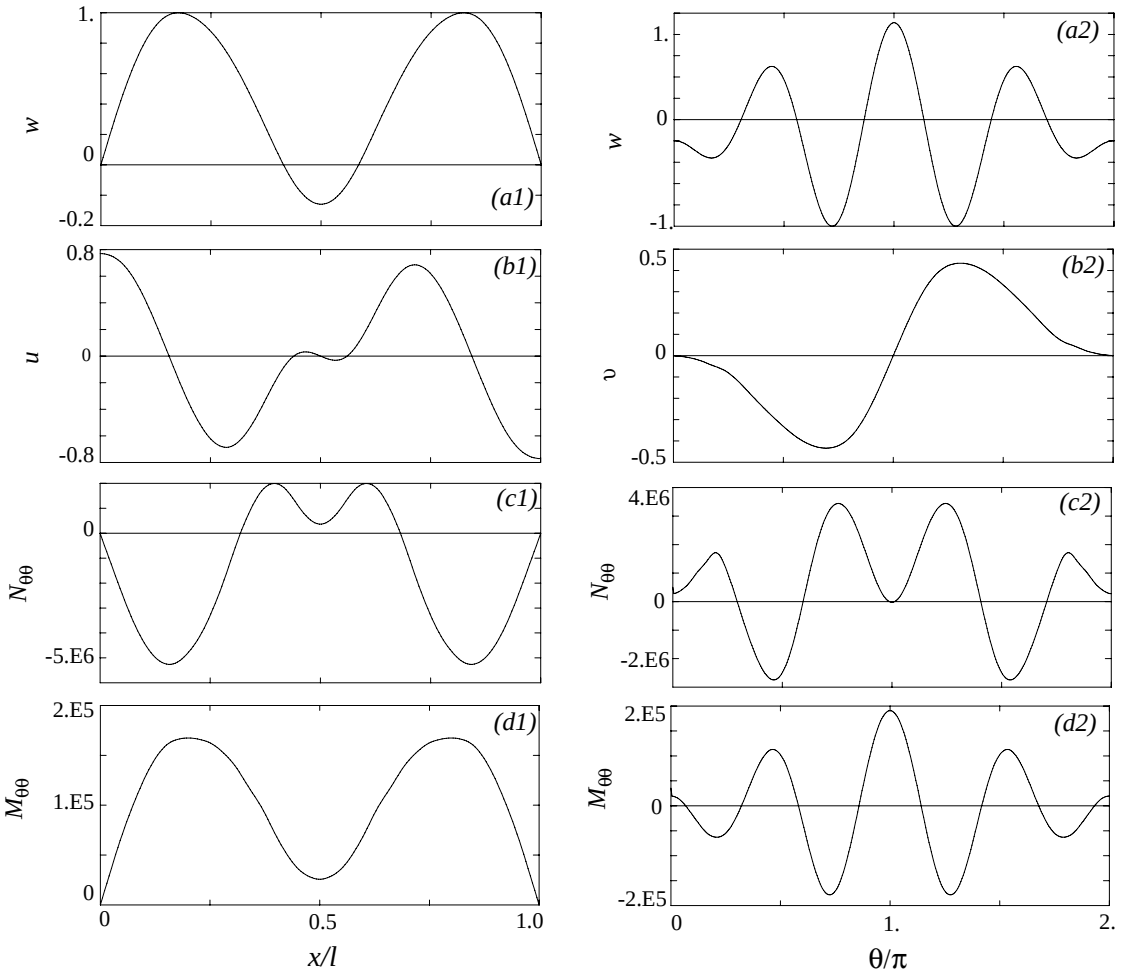

Fig. 6. Coupled modal variables at $\Omega = 3.01$ KHz—$\alpha = 0.8$, $\beta = 5$, $d_f = a\theta_f = 7.62$ cm: (a1)–(d1) along x at $\theta = 0$, (a2)–(d2) along θ at $x = l/2$.

(Figs. 9(a1) and 3(a1)), flexural stresses by 30% (Figs. 9(b1) and (c1) and 3(b1) and (c1)), while extensional stresses are higher by a factor of 3 (Figs. 9(b2) and (c2) and 3(b2) and (c2)) consistent with the increased modal u and υ. An explanation is that local resonant frequencies in the patch are denser due to the lower modulus. Conditions of anti-resonance are then more probable explaining this apparent inertial rigidity although statically the patch is weaker.

Fig. 10 plots histories of the inhomogeneous cylinder at $y/r_p = 0, 3, 6, 9$ along $x_c = 0$. Remote from impact $y/r_p = 9$, the magnitude of w is as large as at the center of impact $y/r_p = 0$. All other variables resemble those in Fig. 9. As with the homogeneous cylinder, response is not axially symmetric about the center of impact.

Consider a disk with the same properties, plate thickness, footprint radius, modulus inhomogeneity and forcing pulse as those of the cylinder. The disk radius r_d is taken half the length of the cylinder $l/2$. The inhomogeneous patch is a concentric circle with radius $r_f = d_f$. Fig. 11 plots $E(r)$ from (22c) for the inhomogeneous disk. Fig. 11(a) shows one method with constant Δr discretization for $0 \leqslant r \leqslant r_f$, while Fig.

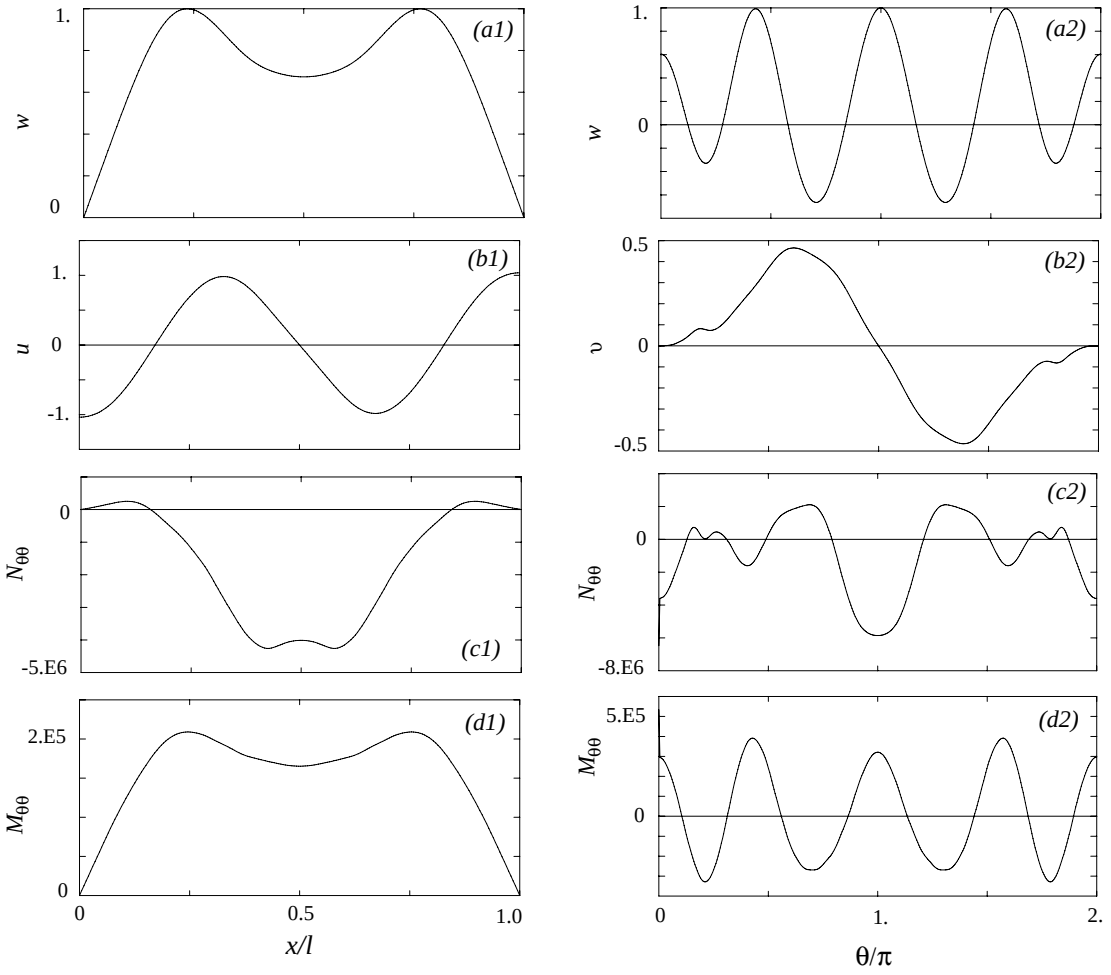

Fig. 7. Coupled modal variables at $\Omega = 3.39$ KHz—$\alpha = 0.8$, $\beta = 5$, $d_f = a\theta_f = 7.62$ cm: (a2)–(d2) along x at $\theta = 0$, (a2)–(d2) along θ at $x = l/2$.

11(b) shows another with a constant ΔE discretization. Numerical experiments indicate that results are insensitive to the method of discretization.

Fig. 12 plots histories of the disk. Three cases are considered: a disk with $E = E_0$ (Fig. 12(a1)–(c1)), a disk with $E = E(0)$ (Fig. 12(a2)–(c2)), and an inhomogeneous disk with $E = E(r)$ as in (22c) (Fig. 12(a3)–(c3)). Axial displacement w and flexural stresses σ_{rr} and $\sigma_{\theta\theta}$ are similar in shape for the three cases. w rises reaching a plateau at $t = \Delta t_f$ which is disturbed at the time when reflection from the boundary $r = r_d$ reaches that station. Since $E_0 = 5E(0)$, the time delay for the wave to propagate from the footprint to some station remote from impact is longer by a factor of $\sqrt{5}$ as shown in Fig. 12(a1) and (a2), noting that phase velocity scales as $\sqrt{E}$. Magnitude of w in Fig. 12(a2) is 30% larger than that in Fig. 12(a1). In Fig. 12(a3) $w(0)$ has the same magnitude as that in Fig. 12(a2) since near the start, magnitude depends on local properties and those match for cases 2 and 3 for $r \leqslant r_f$. For $t > \Delta t_f$, w diminishes smoothly to reach a lower plateau consistent with case 1 (Fig. 12(a1)). Flexural stresses (Fig. 12(b1)–(b3) and (c1)–(c3)) are comparable for the three cases and reach magnitudes approximately those of the homogeneous cylinder (Fig. 3(b1) and

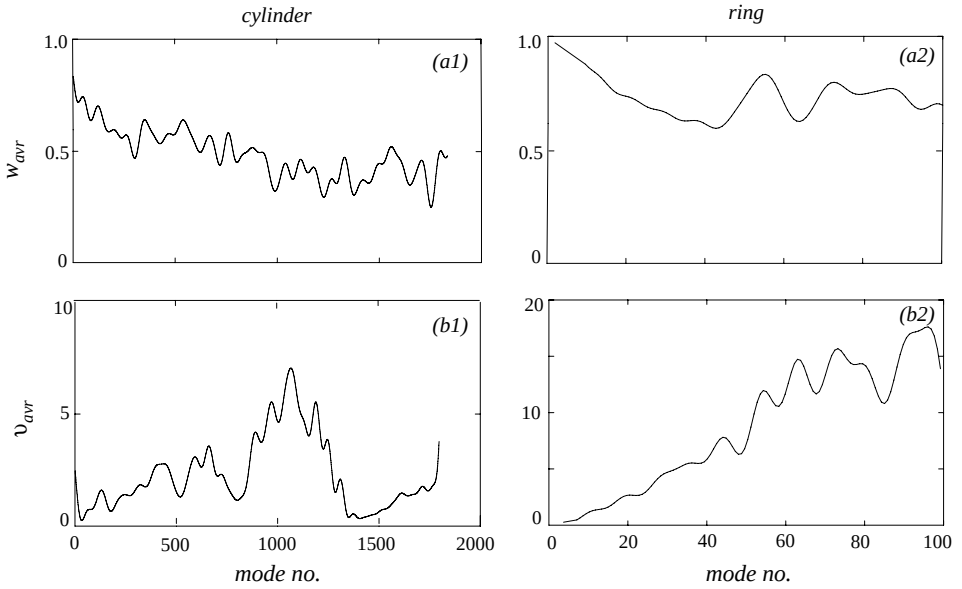

Fig. 8. Normalized displacement averages ($\alpha = 0.8$, $\beta = 5$)—(a1) and (b1) cylinder: $d_f = a\theta_f = 7.62$ cm; (a2) and (b2) ring: $a\theta_f = 7.62$ cm.

(c1)) and Fig. 4(b1) and (c1)). For the disk, reflections from the edge $r = r_d$ produce strong fluctuations in response because, in radiating from the center of impact, each wave front is reflected from the edge at the same time producing a condition of the reflected waves called coherence. This is absent for the cylinder due to curvature and asymmetry of the boundaries with respect to center of impact (Fig. 3(b1) and (c1)).

Histories of the homogeneous ring are shown in Fig. 13(a1)–(d1) and those of the inhomogeneous ring in Fig. 13(a2)–(d2). For the homogeneous ring, w and $\sigma_{\theta\theta f}$ are more than three times those of the cylinder while $\sigma_{\theta\theta e}$ is comparable (Fig. 4). Inhomogeneity in the ring increases w by a factor of 2, and reduces $\sigma_{\theta\theta f}$ by a factor of 2, and $\sigma_{\theta\theta e}$ by a factor of 7. The only resemblance with the inhomogeneous cylinder is that remote from impact and close to the inhomogeneous patch magnitudes of w and $\sigma_{\theta\theta e}$ are comparable to those at the center of impact (Fig. 13(a2), (c2) and (d2) and Fig. 10(a1), (c1) and (c2)). The reason for this large difference between ring and cylinder is that the ring can also be viewed as a cylinder when axial dimensions of cylinder, inhomogeneous patch and footprint tend to infinity. The extended length of the footprint increases the excitation force which in turn raises w. All stresses are reduced because axial curvature and u vanish.

A closer approach of cylinder response to the ring's might be by extending patch length $2d_f$ and footprint length d_{px} to 48.3 cm which is almost the full length of the cylinder, while keeping patch width $2\theta_{f\,\mathrm{a}}$ and footprint width d_{py} the same. Therefore Fig. 14 plots the smoothed distribution of u_{avr},υ_{avr} and w_{avr} for this more "ring-like" cylinder. However, Fig. 14(a) shows that u_{avr} does not diminish towards the vanishing limit of the ring. Moreover, w_{avr} follows the trend in Fig. 8(a1) with a slight increase in magnitude. This suggests that the cylinder's extensional stresses may increase accounting for the deviation from the expected trend of the ring.

Fig. 15 plots histories of this cylinder at $y/r_p = 0, 3, 6, 9$ along $x_c = 0$. Comparing these histories with Fig. 10, note that except for σ_{xxf}, σ_{xxe} and $\sigma_{\theta\theta f}$ increase by a factor of 5 and $\sigma_{\theta\theta e}$ increases by an order of magnitude. It appears that the cylinder's $l/a = 4$ is still not high enough to approximate the ring's state of plane stress when axial dependence vanishes.

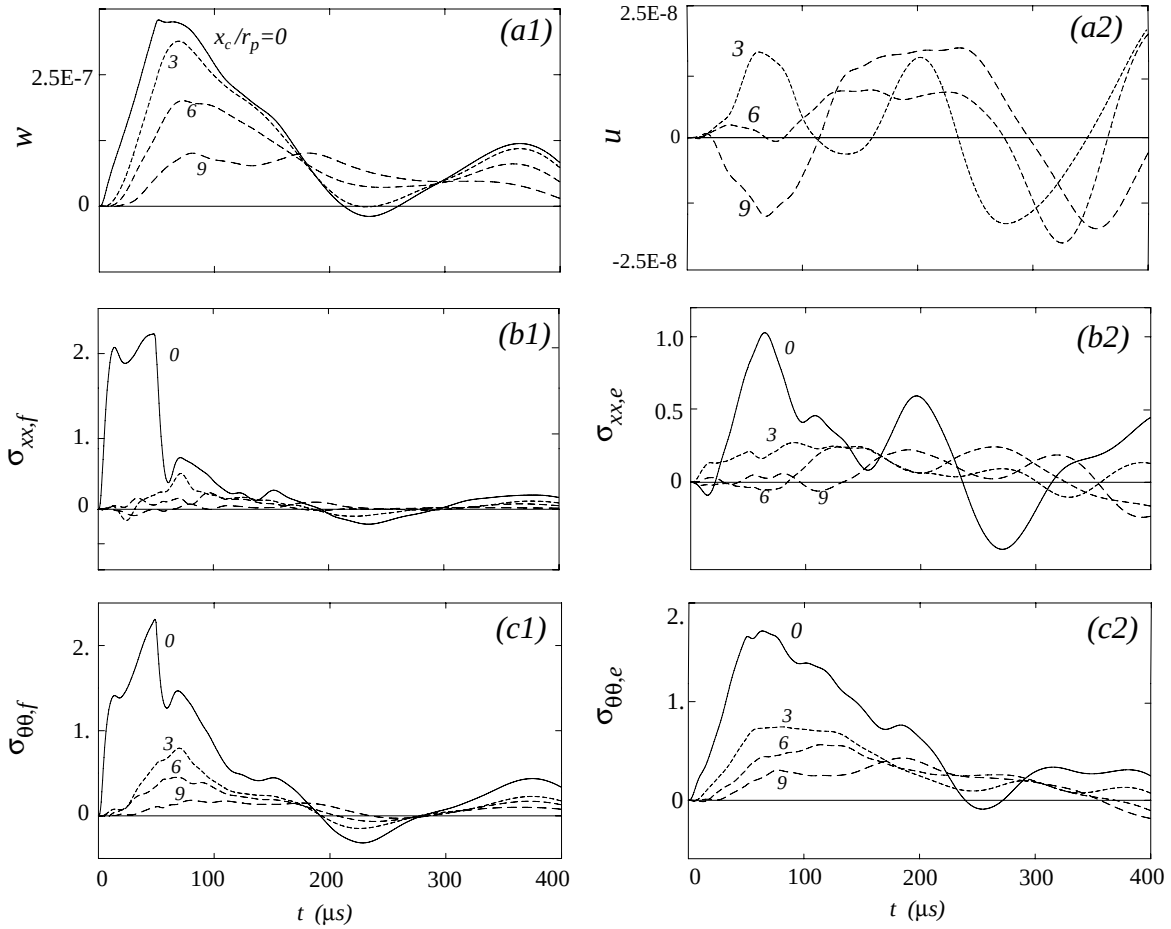

Fig. 9. Histories of cylinder at $y = 0$, $\alpha = 0.8$, $\beta = 5$, $d_f = a\theta_f = 7.62$ cm: —— $x_c/r_p = 0$, ---- 3, –– 6, —— 9.

6. Conclusion

The Galerkin method was employed to analyze wave propagation in a thin cylinder with material inhomogeneity within a rectangular patch over its surface. Limiting cases of the disk and ring were also analyzed with a view to find a simpler but consistent approximation to treat inhomogeneity. Noteworthy features of local inhomogeneity on response are:

(1) Except for isolated modes, resonant frequencies of the cylinder are not affected. In contrast, modal quantities differ substantially from those of the homogeneous cylinder.
(2) In the patch,
   (i) w, σ_{xxf}, $\sigma_{\theta\theta f}$ are reduced while σ_{xxe}, $\sigma_{\theta\theta e}$ increase substantially.
   (ii) w is substantially smaller than $w_{\max}$.
   (iii) u and υ are larger affecting σ_{xxe}, $\sigma_{\theta\theta e}$.
(3) Normalized average modal displacements are reliable measures of stress response magnitude.
(4) Except for magnitude of σ_{rr} and $\sigma_{\theta\theta}$ at first arrival, the disk poorly approximates the cylinder as it lacks the extensional contribution.

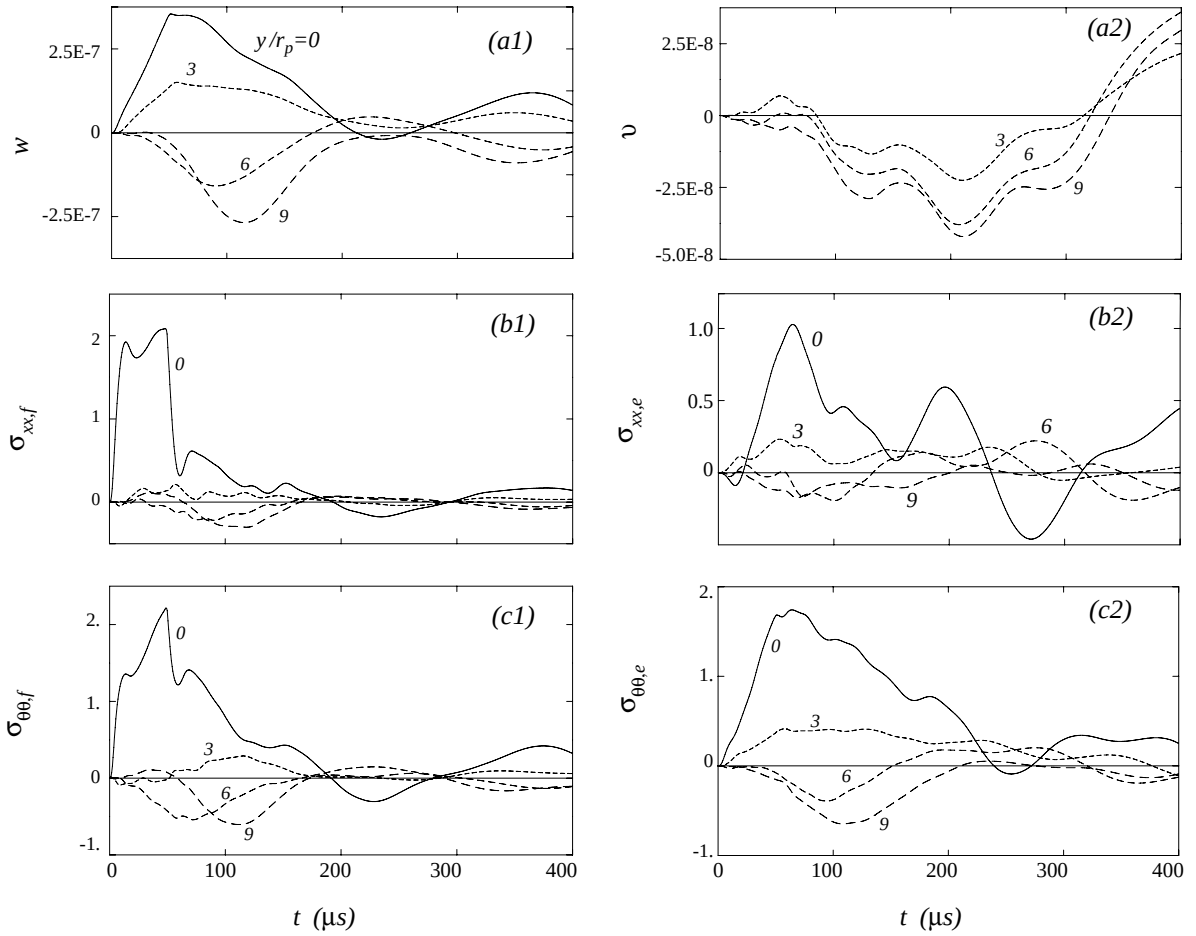

Fig. 10. Histories of cylinder at $x_c/r_p = 0$, $\alpha = 0.8$, $\beta = 5$, $d_f = a\theta_f = 7.62$ cm: —— $y/r_p = 0$, ---- 3, –– 6, —— 9.

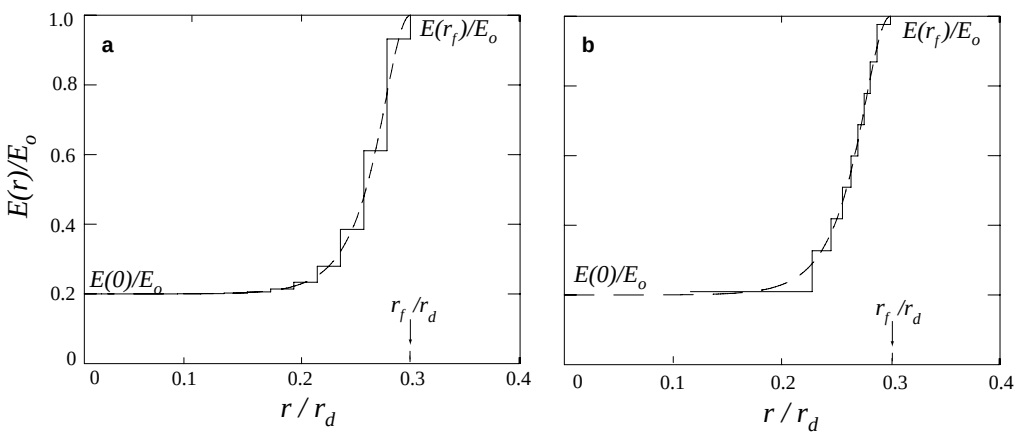

Fig. 11. $E(r)$ profile—$\alpha = 0.8$, $\beta = 5$: (a) constant Δr, (b) constant ΔE; ---- actual, —— step discretization.

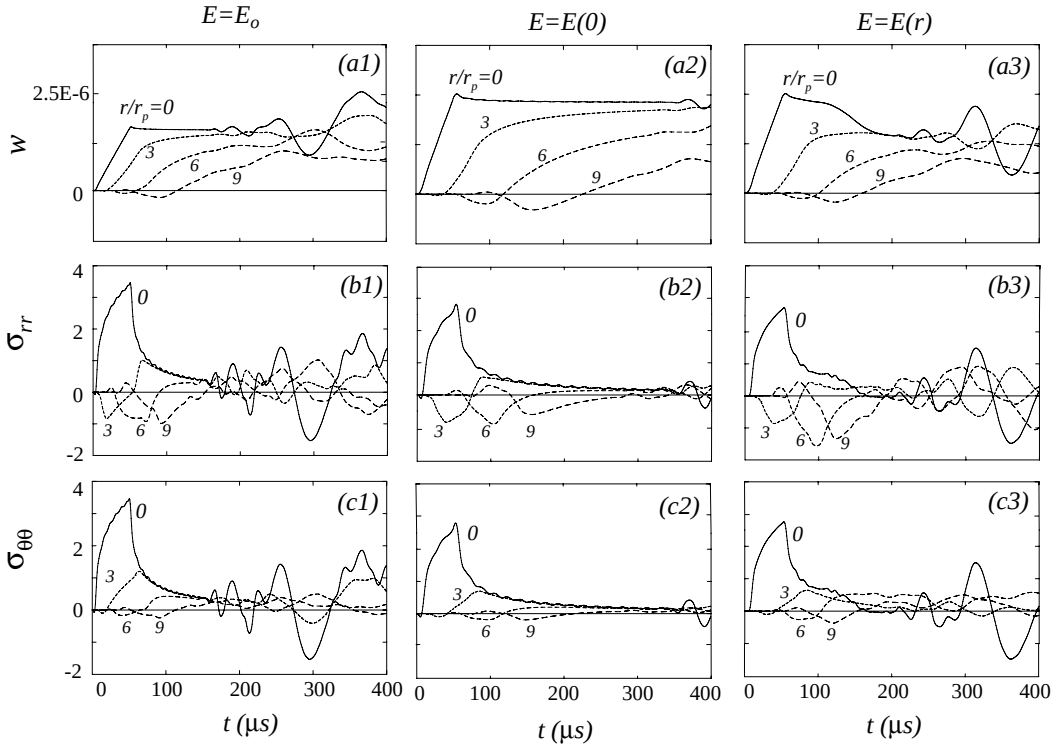

Fig. 12. Histories of disk: (a1)–(c1) $E = E_0$; (a2)–(c2) $E = E_0$; (a3)–(c3) $E = E_r$, $r_f = 7.62$ cm.

(5) The ring is weaker than the cylinder as it lacks axial stiffness and an increase in external excitation. This can be explained by viewing the ring as a cylinder when all axial dimensions extend to infinity.
(6) Neither disk nor ring possess the relevant features of the cylinder and therefore are not candidates for supplying a consistent approximation to the cylinder. The disk lacks curvature coupling extensional to flexural motions and the ring lacks stiffness imposed by axial dependence.
(7) Even when patch and footprint lengths are extended to cylinder's length, a ratio of $l/a = 4$ is not high enough to approximate the ring's state of plane stress. This demonstrates how sensitive extensional stresses are to axial displacement.

Appendix A. Shear deformation factor

For a thin cylinder and harmonic motions in time, Mindlin's (1951) flexural equation is identical to the plate's equation namely

$$[\nabla^2 + (\rho/\kappa G)\omega^2][D\nabla^2 + (\rho h^3/12)\omega^2]w - \rho h\omega^2 = 0$$
$$\nabla^2 \equiv \partial_{xx} + 1/a^2\partial_{\theta\theta} \tag{A1}$$

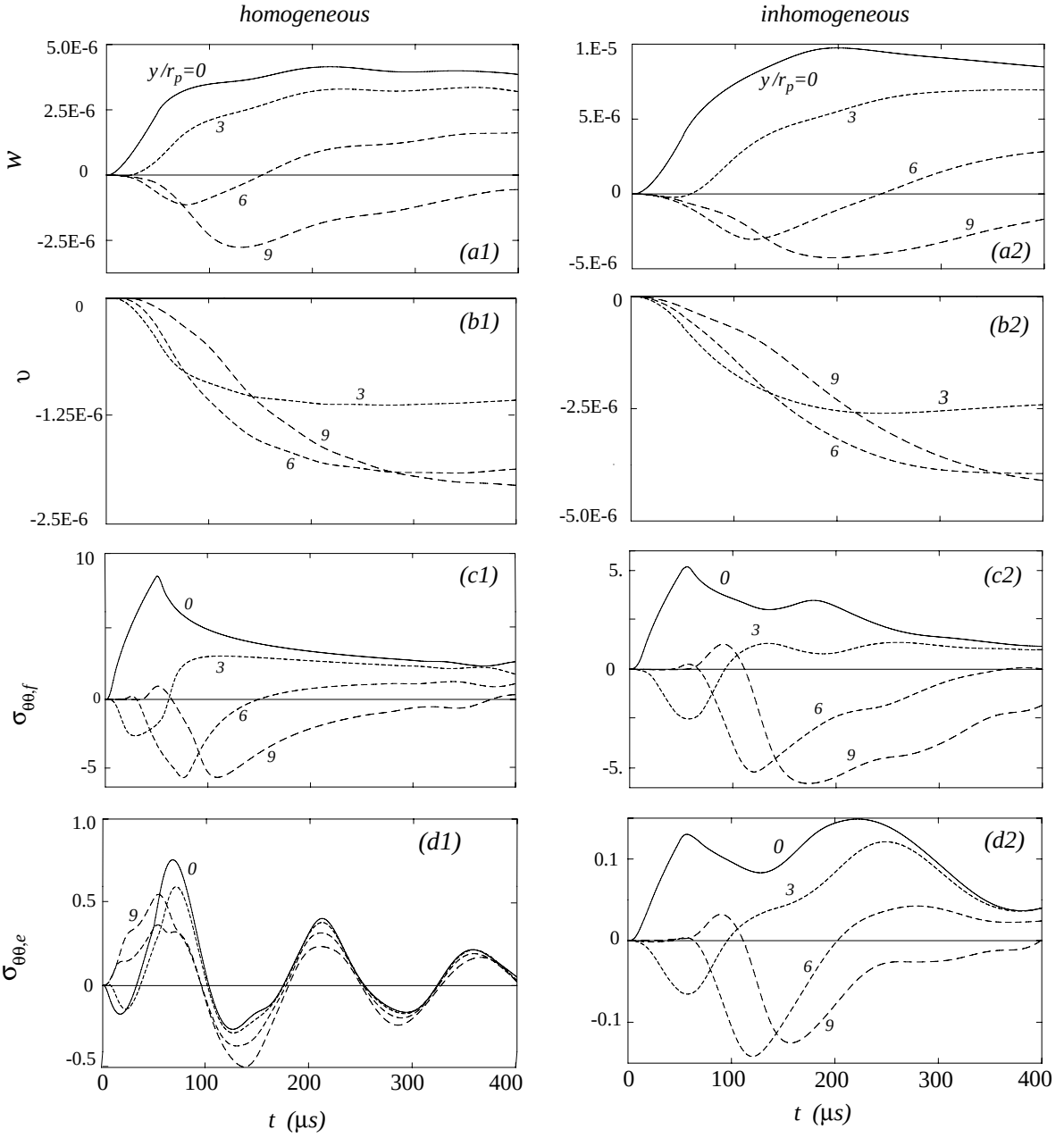

Fig. 13. Histories of ring: (a1)–(d1) homogeneous; (a2)–(d2) $\alpha = 0.8$, $\beta = 5$, $a\theta_f = 7.62$ cm; —— $y/r_p = 0$, ---- 3, –– 6, —— 9.

(x, θ) are axial and circumferential coordinates, w is radial displacement, h is wall thickness, $D = E_0 h^3/12(1 - \nu^2)$ is flexural rigidity, (E_0, G) are Young's and shear moduli, ν is Poisson's ratio, κ is shear constant, and ρ is density. For simply supported boundary conditions, an exact solution exists in the form

$$w(x, \theta) = w_0 \sin(s_m x)\cos(n\theta), \quad s_m = m\pi/l \tag{A2}$$

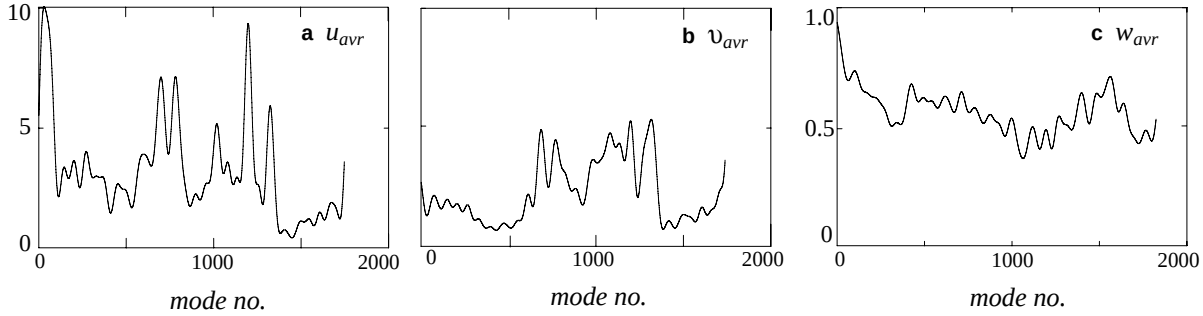

Fig. 14. Normalized displacement averages of cylinder: $\alpha = 0.8$, $\beta = 5$, $a\theta_f = 7.62$ cm, $d_f = 24.1$ cm.

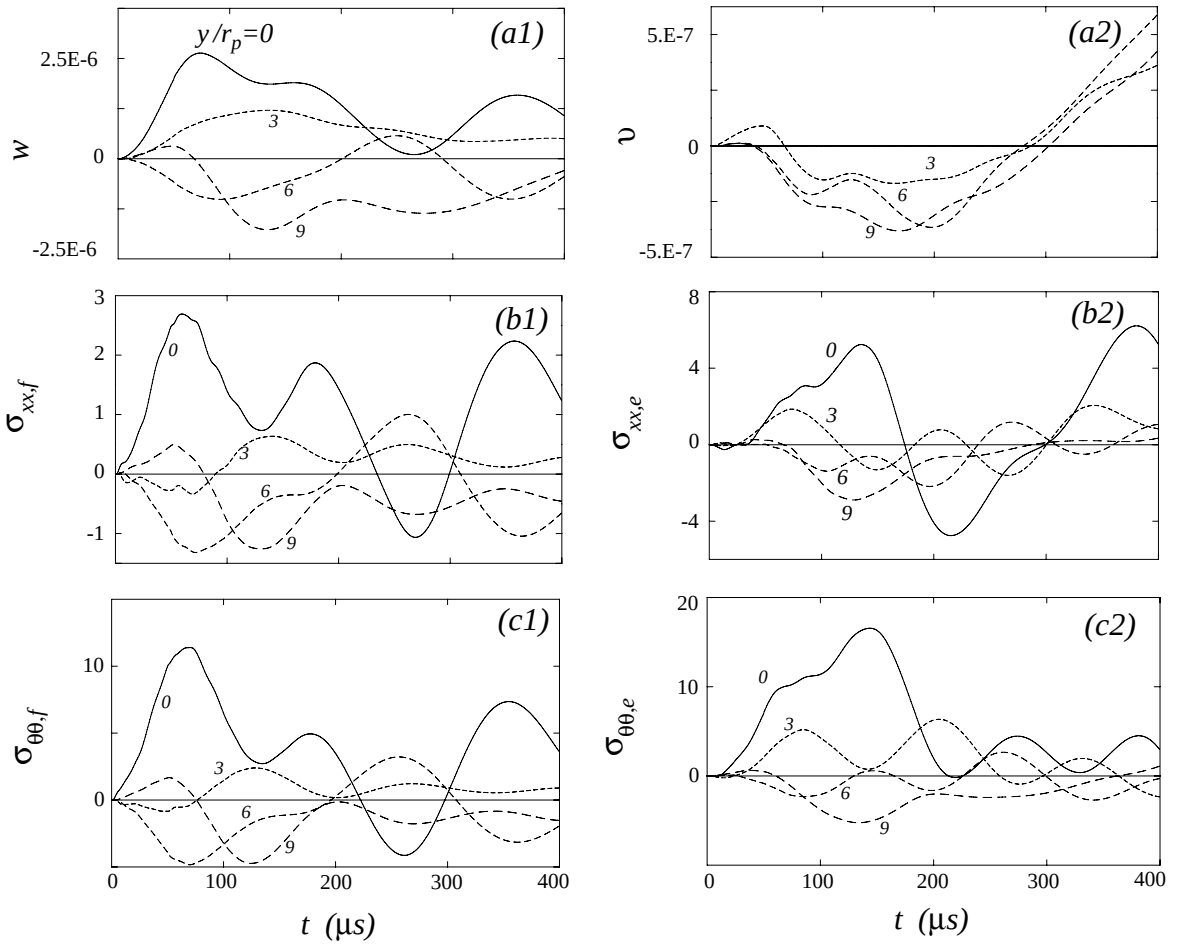

Fig. 15. Histories of cylinder at $x_c/r_p = 0$: $\alpha = 0.8$, $\beta = 5$, $a\theta_f = 7.62$ cm; —— $y/r_p = 0$, ---- 3, ––– 6, —— 9.

(n, m) are circumferential and axial wave-numbers, and l and a are cylinder length and radius. Substituting (A2) in (A1) produces the dispersion relation

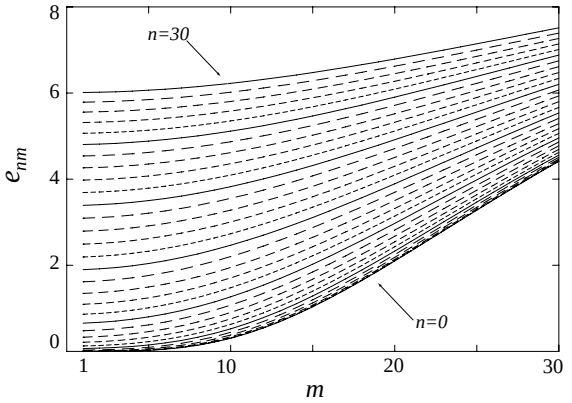

Fig. A.1. % Error in Ω_{nm} from shear factor approximation.

$$\omega_0^2\tilde{r}^2(\bar{s}_m^2+n^2)^2-\omega^2[1+\chi\tilde{r}^2(\bar{s}_m^2+n^2)-(\omega/\omega_s)^2]=0 \tag{A3}$$

$$\bar{s}_m=as_m,\quad \chi=1+E_0/\kappa G(1-\nu^2)=1+2/\kappa(1-\nu)$$
$$\tilde{r}=h/\sqrt{12}a,\quad \omega_s=\sqrt{12\kappa G/\rho}/h,\quad \omega_0=\sqrt{E_0/\rho(1-\nu^2)}/a$$

(ω_0,ω_s) are ring and shear frequencies. The term $\omega^2\tilde{r}^2(\bar{s}_m^2+n^2)$ in (A3) represents rotary inertia. For $h/a\ll 1$ then $(\omega_0/\omega_s)^2=2\tilde{r}^2/\kappa(1-\nu)\ll 1$, and for $\omega=\mathrm{O}(\omega_0)$ then

$$(\omega/\omega_s)^2\approx 2\tilde{r}^2/\kappa(1-\nu)\ll 1+\chi\tilde{r}^2(\bar{s}_m^2+n^2) \tag{A4}$$

This implies that in (A3) $(\omega/\omega_s)^2$ can be neglected compared to the other terms yielding a consistent approximation to the eigenfrequency

$$\omega_{nm}\simeq\omega_0\tilde{r}(\bar{s}_m^2+n^2)\Big/\sqrt{1+\chi\tilde{r}^2(\bar{s}_m^2+n^2)} \tag{A5}$$

Since in (A5) the term $\tilde{r}^2(\bar{s}_m^2+n^2)$ in the denominator represents rotary inertia, then (A5) suggests that shear deformation may be included in Koiter's (1960) shell equations by multiplying rotary inertia by χ. Fig. A.1 plots the error $e_{nm}=100((\omega_{\text{exact}}-\omega_{\text{approx}})/\omega_{\text{exact}})_{nm}$ committed in the flexural resonances by this approximation versus m with n as parameter for a cylinder with the following properties:

$$a=12.7\text{ cm }(=5\text{ in.}),\quad h=1.27\text{ cm }(=0.5\text{ in.}),\quad l=50.8\text{ cm }(=20\text{ in.})$$
$$E_0=2.07\times10^{12}\text{ dyn/cm}^2\ (=30\times10^6\text{ psi}),$$
$$\rho=8\text{ g/cm}^3\ (=7.5\times10^{-4}\text{ lbs}^2/\text{in.}^4),\quad \nu=0.3$$

and for $0\leqslant n\leqslant 30$ and $1\leqslant m\leqslant 30$. ω_{exact} is determined from relation (A3), and ω_{approx} from (A5). In this range, e_{nm} rises gradually with m and n but remains small (<8%) confirming the validity of the approximation.

Appendix B. Stiffness matrix coefficients of inhomogeneous cylinder

In the coefficients defined in (B.1–B.6), superscript i_1 in $C_{mn,jk}^{(i_1 i_2)}$ refers to the equation number of its origin where $i_1=1,2,3$ corresponds to (15a), (15b) and (15c) respectively, and superscript $i_2=1,2,3,4$ refers to

the term number in that equation. Each term multiplies a specific (x, θ) trigonometric function. Superscripts and subscripts of $I_{i_1}^{(x_p x_q)}$ are demonstrated in an example; e.g. $I_3^{(x\theta)}$ originates from the 3rd Eq. (15c) and includes the derivative $\partial_{x\theta} E(x, \theta)$. Also, define $h_1 = h/(1 - v^2)$ and $h_2 = h^3/12(1 - v^2)$,

$$C_{mn,jk}^{(11)} = h_1[(s_j^2 + (1 - v)(k/a)^2/2)u_{kj} + (1 + v)s_j k/2a v_{kj} + v s_j/a w_{kj}]u_{nm} I_1^{(0)} \tag{B1a}$$

$$C_{mn,jk}^{(12)} = h_1(1 - v)/2a(k/a u_{kj} + s_j v_{kj})u_{nm} I_1^{(\theta)} \tag{B1b}$$

$$C_{mn,jk}^{(13)} = h_1(s_j u_{kj} + v k/a v_{kj} + v/a w_{kj})u_{nm} I_1^{(x)} \tag{B1c}$$

$$\begin{aligned} C_{mn,jk}^{(21)} = {} & \{h_1(1 + v)s_j k/2a u_{kj} + [h_1((1 - v)s_j^2/2 + (k/a)^2) + h_2(2(1 - v)s_j^2 + (k/a)^2)/a^2]v_{kj} \\ & + k[h_2((2 - v)s_j^2 + (k/a)^2) + h_1]/a^2 w_{kj}\} v_{nm} I_2^{(0)} \end{aligned} \tag{B2a}$$

$$C_{mn,jk}^{(22)} = -[h_1(1 - v)k/2a u_{kj} + (1 - v)s_j(h_1/2 + 2h_2/a^2)v_{kj} + 2h_2(1 - v)s_j k/a^2 w_{kj}]v_{nm} I_2^{(x)} \tag{B2b}$$

$$C_{mn,jk}^{(23)} = -[h_1 v s_j/a u_{kj} + k(h_1 + h_2/a^2)/a^2 v_{kj} + (h_1 + h_2(v s_j^2 + (k/a)^2)/a^2)/a^2 w_{kj}]v_{nm} I_2^{(\theta)} \tag{B2c}$$

$$\begin{aligned} C_{mn,jk}^{(31)} = {} & \{h_1 v s_j/a I_3^{(0)} u_{kj} + [h_2(s_j^4 + (k/a)^4 + 2(s_j n/a)^2)I_3^{(0)} + h_1/a^2 I_3^{(0)} - h_2(s_j^2 + v(k/a)^2)I_3^{(xx)} \\ & - h_2(v s_j^2 + (k/a)^2)I_3^{(\theta\theta)}/a^2]w_{kj} + k[h_1 + h_2((2 - v)s_j^2 + (k/a)^2)I_3^{(0)} - h_2 v I_3^{(xx)} \\ & - h_2 I_3^{(\theta\theta)}/a^2]/a^2 v_{kj}\} w_{nm} \end{aligned} \tag{B3a}$$

$$C_{mn,jk}^{(32)} = -[2h_2(1 - v)s_j(v_{kj} + k w_{kj})/a^2]w_{nm} I_3^{(x\theta)} \tag{B3b}$$

$$C_{mn,jk}^{(33)} = -2h_2 s_j[k v_{kj}/a^2 + (s_j^2 + (k/a)^2)w_{kj}]w_{nm} I_3^{(x)} \tag{B3c}$$

$$C_{mn,jk}^{(34)} = h_2[2((1 - v)s_j^2 + (k/a)^2)v_{kj} + k(s_j^2 + (k/a)^2)w_{kj}]/a^2 w_{nm} I_3^{(\theta)} \tag{B3d}$$

where

$$\begin{aligned} I_1^{(0)} &= a\int_0^l \int_0^{2\pi} E(x,\theta)C_j(x)C_k(\theta)C_m(x)C_n(\theta)\,\mathrm{d}\theta\,\mathrm{d}x \\ I_1^{(x)} &= a\int_0^l \int_0^{2\pi} E_x(x,\theta)S_j(x)C_k(\theta)C_m(x)C_n(\theta)\,\mathrm{d}\theta\,\mathrm{d}x \\ I_1^{(\theta)} &= a\int_0^l \int_0^{2\pi} E_\theta(x,\theta)C_j(x)S_k(\theta)C_m(x)C_n(\theta)\,\mathrm{d}\theta\,\mathrm{d}x \end{aligned} \tag{B4}$$

$$\begin{aligned} I_2^{(0)} &= a\int_0^l \int_0^{2\pi} E(x,\theta)S_j(x)S_k(\theta)S_m(x)S_n(\theta)\,\mathrm{d}\theta\,\mathrm{d}x \\ I_2^{(x)} &= a\int_0^l \int_0^{2\pi} E_x(x,\theta)C_j(x)S_k(\theta)S_m(x)S_n(\theta)\,\mathrm{d}\theta\,\mathrm{d}x \\ I_2^{(\theta)} &= a\int_0^l \int_0^{2\pi} E_\theta(x,\theta)S_j(x)C_k(\theta)S_m(x)S_n(\theta)\,\mathrm{d}\theta\,\mathrm{d}x \end{aligned} \tag{B5}$$

$$
\begin{aligned}
I_3^{(0)} &= a\int_0^l\int_0^{2\pi} E(x,\theta)S_j(x)C_k(\theta)S_m(x)C_n(\theta)\,\mathrm{d}\theta\,\mathrm{d}x\\
I_3^{(x)} &= a\int_0^l\int_0^{2\pi} E_x(x,\theta)C_j(x)C_k(\theta)S_m(x)C_n(\theta)\,\mathrm{d}\theta\,\mathrm{d}x\\
I_3^{(\theta)} &= a\int_0^l\int_0^{2\pi} E_\theta(x,\theta)S_j(x)S_k(\theta)S_m(x)C_n(\theta)\,\mathrm{d}\theta\,\mathrm{d}x\\
I_3^{(xx)} &= a\int_0^l\int_0^{2\pi} E_{xx}(x,\theta)S_j(x)C_k(\theta)S_m(x)C_n(\theta)\,\mathrm{d}\theta\,\mathrm{d}x\\
I_3^{(\theta\theta)} &= a\int_0^l\int_0^{2\pi} E_{\theta\theta}(x,\theta)S_j(x)C_k(\theta)S_m(x)C_n(\theta)\,\mathrm{d}\theta\,\mathrm{d}x\\
I_3^{(x\theta)} &= a\int_0^l\int_0^{2\pi} E_{x\theta}(x,\theta)C_j(x)S_k(\theta)S_m(x)C_n(\theta)\,\mathrm{d}\theta\,\mathrm{d}x
\end{aligned}
\tag{B6}
$$

All integrals in B4,B5B6 which include derivatives of $E(x,\theta)$ vanish everywhere except over the area $x_f-\sqrt{d_f^2-(a\theta)^2}\leqslant x\leqslant x_f+\sqrt{d_f^2-(a\theta)^2}$ and $-\theta_f\leqslant\theta\leqslant\theta_f$. To simplify the numerical evaluation of these integrals $E(x,\theta)$ is extended to cover the square area $x_f-d_f\leqslant x\leqslant x_f+d_f$, $-\theta_f\leqslant\theta\leqslant\theta_f$ with $E(x,\theta)=E_0$ over the intervals

$$
x_f-d_f\leqslant x\leqslant x_f-\sqrt{d_f^2-(a\theta)^2}\quad\text{and}\quad x_f+\sqrt{d_f^2-(a\theta)^2}\leqslant x\leqslant x_f-d_f
$$

Also, each integral can be expressed as the sum of three parts, the first two parts are evaluated analytically and the last part numerically. As an example

$$
I_3^{(0)} = a\int_0^l\int_0^{2\pi} E(x,\theta)S_j(x)C_k(\theta)S_m(x)C_n(\theta)\,\mathrm{d}\theta\,\mathrm{d}x = I_{3,1}^{(0)}-I_{3,2}^{(0)}+I_{3,3}^{(0)}
$$

$$
I_{3,1}^{(0)} = aE_0\int_0^l\int_0^{2\pi} S_j(x)C_k(\theta)S_m(x)C_n(\theta)\,\mathrm{d}\theta\,\mathrm{d}x = E_0\pi al(1+\delta_{n0})\delta_{nk}\delta_{mj}/2
$$

$$
\begin{aligned}
I_{3,2}^{(0)} &= aE_0\int_{x_f-d_f}^{x_f+d_f}\int_{-\theta_f}^{\theta_f} S_j(x)C_k(\theta)S_m(x)C_n(\theta)\,\mathrm{d}\theta\,\mathrm{d}x\\
&= E_0al[(S_{m-j}(x_f)-S_{m-j}(x_f-d_f))/(m-j)-(S_{m+j}(x_f)-S_{m+j}(x_f-d_f))/(m+j)]/\pi\\
&\quad\cdot[S_{n-k}(\theta_f)/(n-k)+S_{n+k}(\theta_f)/(n+k)]
\end{aligned}
$$

$$
S_{m-j}(x)=\sin((m-j)\pi x/l),\quad S_{n-k}(\theta)=\sin((n-k)\theta),\quad\text{etc.}
$$

$$
I_{3,3}^{(0)} = a\int_{x_f-d_f}^{x_f+d_f}\int_{-\theta_f}^{\theta_f} E(x,\theta)S_j(x)C_k(\theta)S_m(x)C_n(\theta)\,\mathrm{d}\theta\,\mathrm{d}x
$$

$I_{3,1}^{(0)}$ is over the entire cylinder when $E=E_0$, $I_{3,2}^{(0)}$ is over the patch when $E=E_0$, and $I_{3,3}^{(0)}$ is over the patch when $E=E(x,\theta)$.

Appendix C. Inhomogeneous ring

In the limit as cylinder length tends to zero, the x-dependence in Eqs. (1) and (2a) vanishes yielding the ring equations

$$\begin{aligned} &1/a\partial_\theta N_{\theta\theta} - Q_\theta/a = \rho h \partial_{tt} v \\ &1/a\partial_\theta Q_\theta + 1/a N_{\theta\theta} = \rho h \partial_{tt} w + p_w(\theta) f_w(t) \end{aligned} \tag{C1}$$

$$\begin{aligned} &Q_\theta = 1/a\partial_\theta M_{\theta\theta} + \frac{\rho h^3 \chi}{12a}(\partial_{\theta tt} w + \partial_{tt} v) \\ &N_{\theta\theta} = N_0(\partial_\theta v - w)/a, \quad M_{\theta\theta} = -M_0(\partial_{\theta\theta} w - \partial_\theta v)/a^2 \end{aligned}$$

Since (C1) has constant coefficients, it has an exact solution in terms of exponentials. For harmonic motions in time with radian frequency ω,

$$v(\theta,t) = \sum_{j=1}^{6} v_j e^{\alpha_j \theta} e^{i\omega t}, \quad w(\theta,t) = \sum_{j=1}^{6} w_j e^{\alpha_j \theta} e^{i\omega t}, \qquad i = \sqrt{-1} \tag{C2}$$

Substituting (C2) in (C1) yields the sixth order polynomial

$$\sum_{k=0}^{3} c_k \alpha^{2k} = 0 \tag{C3}$$

$$\begin{aligned} &c_3 = N_0 M_0/a^6, c_2 = \rho h\omega^2(N_0\chi^2 + M_0/a^2)/a^2 + 2N_0M_0/a^6 \\ &c_1 = \rho h\omega^2(-M_0/a^4 + \rho h\omega^2\chi^2 - N_0(1-2\chi^2)/a^2)/a^2 + N_0M_0/a^6 \\ &c_0 = \rho h\omega^2(1+\chi^2)(N_0/a^2 - \rho h\omega^2) \end{aligned}$$

Assume a modulus inhomogeneity along θ symmetric about $\theta = 0$ of the form

$$\begin{aligned} &E(\theta) = E_0\{1 - \alpha[1 - \operatorname{sech}(\beta a(\theta+\theta_f)) - \operatorname{sech}(\beta a(\theta-\theta_f))]\}\Theta(\theta) \\ &\Theta(\theta) = H(\theta+\theta_f) - H(\theta-\theta_f), \quad -\theta_f \leqslant \theta \leqslant \theta_f \end{aligned} \tag{C4}$$

and $E(\theta) = E_0$ everywhere else. In (C4) all parameters are defined in Eq. (12) of the text. For an excitation symmetric about $\theta = 0$, motions are also symmetric about $\theta = 0$. Divide the part of the circumference $0 \leqslant \theta \leqslant \pi$ into m_s arc segments $\theta_j \leqslant \theta \leqslant \theta_{j+1}, 1 \leqslant j \leqslant m_s + 1$, where $\theta_1 = 0$ and $\theta_{m_s+1} = \pi$. Assume a stepwise distribution in modulus $E_1, \ldots, E_j, \ldots, E_{m_s}$ where E_j applies to segment $\theta_j \leqslant \theta \leqslant \theta_{j+1}$. Substituting (C2) in (C1) and defining

$$\mathbf{f}_j = \{N_{\theta\theta}, Q_\theta, M_{\theta\theta}\}_j^{\mathrm{T}}, \quad \mathbf{g}_j = \{v, w, w_\theta\}_j^{\mathrm{T}} \tag{C5a}$$

yields

$$\mathbf{f}_j = \mathbf{B}_{\mathbf{f}j}\mathbf{C}_j, \quad \mathbf{g}_j = \mathbf{B}_{\mathbf{g}j}\mathbf{C}_j \tag{C5b}$$

$\mathbf{C}_j = \{C_{1j}, C_{2j}, \ldots, C_{6j}\}^{\mathrm{T}}$, $\mathbf{B}_{\mathbf{f}j}$ and $\mathbf{B}_{\mathbf{g}j}$ are 3×6 matrices with coefficients involving the exponential functions in (C2) and their derivatives. Defining the state vector at an interface as $\mathbf{S}_j = \{\mathbf{f}_j, \mathbf{g}_j\}^{\mathrm{T}}$, evaluating (C5b) at the two ends of segment j then eliminating $\mathbf{C}_j$ determines the transfer matrix of the jth segment relating $\mathbf{S}_j(\theta_j)$ to $\mathbf{S}_j(\theta_{j+1})$

$$\begin{aligned} &\mathbf{S}_j(\theta_{j+1}) = \mathbf{T}_{j,j+1}\mathbf{S}_j(\theta_j) \equiv \mathbf{B}_{\mathbf{s}j}^{-1}(\theta_j)\mathbf{B}_{\mathbf{s}j}(\theta_{j+1})\mathbf{S}_j(\theta_j) \\ &\mathbf{B}_{\mathbf{s}j} = \begin{bmatrix} \mathbf{B}_{\mathbf{f}j} \\ \mathbf{B}_{\mathbf{g}j} \end{bmatrix} \end{aligned} \tag{C6}$$

Enforcing continuity of $\mathbf{f}_j$ and $\mathbf{g}_j$ at interfaces of segments and symmetry conditions at $\theta = 0$ and $\theta = \pi$ produces a set of $m_s + 1$ tri-diagonal block matrices in the interface state vectors $\mathbf{S}_j$. For the case of 3 arc segments, the tri-diagonal block system is similar in form to the global transfer matrix (31) except that all submatrices are 3×3 and

(i) The first row $[\mathbf{I} \quad -\mathbf{Z}_0]$ is replaced by $[\mathbf{F}_a \quad \mathbf{G}_a]$.
(ii) The last row $[\mathbf{0} \quad \mathbf{I}]$ is replaced by $[\mathbf{F}_b \quad \mathbf{G}_b]$.

$\mathbf{F}_a$, $\mathbf{G}_a$ and $\mathbf{F}_b$, $\mathbf{G}_b$ are 3×3 symmetry matrices. Since the symmetry condition about $\theta = 0$ and $\theta = \pi$ can be expressed as $Q_\theta = \upsilon = \partial_\theta w = 0$, in turn all elements in $\mathbf{F}_a$ and $\mathbf{F}_b$ are zero except for $\mathbf{F}_{12} = 1$, and all elements in $\mathbf{G}_a$ and $\mathbf{G}_b$ are zero except for $G_{21} = G_{33} = 1$.

From here on, steps leading to transient response are identical to those adopted in Eqs. (32)–(35) for the disk.

References

Bao, X. et al., 1997. The resonances of finite-length elastic cylinders and elastic spheroids excited by sound scattering. Journal of the Acoustical Society of America 102, 49.

Batard, H., Quentin, G., 1992. Acoustical resonances of solid elastic cylinders: parametric study. Journal of the Acoustical Society of America 91, 581.

Cheung, Z., Lo, Y., Au, S., 2003. 3-D vibration analysis of solid and hollow circular cylinders via Chebyshev–Ritz method. Computer Methods in Applied Mechanics and Engineering 192 (13–14), 1575–1589.

El-Raheb, M., 2004. Transient response of a metallic capsule to an internal pressure pulse. International Journal of Solids & Structures 41/18–19, 4899–4918.

El-Raheb, M., Wagner, P., 1985. Harmonic response of cylindrical and toroidal shells enclosing an acoustic medium, Part I: Theory. Journal of the Acoustical Society of America 78, 738–746.

El-Raheb, M., Wagner, P., 1986. Damped response of shells with vibration absorbers. Transactions ASME Journal of Applied Mechanics 53, 902–908.

El-Raheb, M., Wagner, P., 1989a. Acoustic radiation from a shell with internal structures. Journal of the Acoustical Society of America 85, 2452–2464.

El-Raheb, M., Wagner, P., 1989b. Wave propagation in thin cylinders with point masses. Journal of the Acoustical Society of America 85, 759–767.

Grinchenko, V., 1999. Eigenforms and eigenfrequency spectrum of finite elastic cylinder. Journal of the Acoustical Society of America 105, 1392.

Honarvar, F., Sinclair, A., 1996. Acoustic wave scattering from transversely isotropic cylinders. Journal of the Acoustical Society of America 100, 57.

Hussein, M., Heyliger, P., 1998. Three-dimensional vibrations of lavered piezoelectric cylinders. Journal of Engineering Mechanics 124, 1294.

Koiter, W., 1960. A Consistent First Approximation in the General Theory of Thin Elastic Shells, I.U.T.A.M.. North-Holland, Amsterdam.

Lin, C., Jen, M., 2003. Analysis of laminated anisotropic cylindrical shell by Chebyshev collocation method. Transactions ASME Journal of Applied Mechanics 70, 391.

Mindlin, R., 1951. Influence of rotary inertia and shear on flexural motions of isotropic elastic plates. Transactions ASME Journal of Applied Mechanics 73, 31–38.

Paul, H., Murali, V., 1995. Dynamic response of axisymmetric poroelastic cylindrical bone. Journal of the Acoustical Society of America 98 (5), 2978.

Soldatos, K., 1994. Review of three-dimensional dynamic analyses of circular cylinders and cylindrical shells. ASME Applied Mechanics Reviews 47 (10), 501–516.

Soldatos, K., Ye, J., 1994. Wave propagation in anisotropic laminated hollow cylinders of infinite extent. Journal of the Acoustical Society of America 96 (6), 3744–3752.

Stanton, T., 1988. Sound scattering by cylinders of finite length. II. Elastic cylinders. Journal of the Acoustical Society of America 83, 64.

Stepanishen, P., Janus, R., 1990. Transient radiation and scattering from fluid loaded elastic cylinders. Journal of the Acoustical Society of America 88 (Suppl. 1), S78.

Um, C., Liew, K., Kitipornchai, S., 1998. Vibration of open cylindrical shells: a three-dimensional elasticity approach. Journal of the Acoustical Society of America 104, 1436.
Wang, C., Swaddiwudhipong, S., Tian, J., 1997. Ritz method for vibration analysis of cylindrical shells with ring stiffeners. Journal of Engineering Mechanics 123, 134.
Wang, X., Ying, C., 2001. Scattering of Lamb waves by a circular cylinder. Journal of the Acoustical Society of America 110, 1752.